

Teze disertace
k získání vědeckého titulu “doktor věd”
ve skupině věd: fyzikálně-matematické vědy

**Vectorized implementations of the finite element method
and applications to nonlinear problems**

Komise pro obhajoby doktorských disertací v oboru: Matematická analýza a příbuzné
obory

Jméno uchazeče: Jan Valdman

Pracoviště uchazeče: ÚTIA AV ČR, v.v.i.

Místo a datum: Praha, 2. 12. 2024

Contents

1	Introduction	3
2	Linear problems	6
2.1	Diffusion-reaction problem	7
2.2	Linear elasticity	8
2.3	Eddy-current problem	10
2.4	FEM assemblies: implementation concepts	11
3	Linearized and eigenvalue problems	13
3.1	A posteriori error estimate for the Poisson problem	13
3.2	A posteriori error estimate for the two-phase obstacle problem	15
3.3	Elastoplasticity in small strains	17
3.4	Eigenvalue problems	18
4	Nonlinear problems	20
4.1	Hadamard inequality in mean	20
4.2	Non-penetrability of elastic solids	23
4.3	Energy minimizations: implementation concepts	25
5	References	28

1 Introduction

The finite element method (FEM) is an extremely popular numerical method to solve differential equations arising in engineering and mathematical modeling. Typical areas of interest include traditional fields of structural analysis, heat transfer, fluid flow, mass transport, and electromagnetic potential. Its development can be traced back to the work of Alexander Hrennikoff [41] and Richard Courant [20] in the early 1940s. According to a review paper [51], there were four historical time periods:

1. (1941-1965) the birth of the Finite Element Method,
2. (1966-1991) the golden age of the Finite Element Method,
3. (1992-2017) broad industrial applications and materials modeling,
4. (2018-present) the state-of-the-art FEM technology for the current and future eras of FEM research.

It is obvious that there exist a huge number of books and papers on the finite element method, e.g., [9, 8, 21, 29, 74] to name a few suggested for individual studies. An example of a FEM calculation for the two-surface elastoplasticity model from [13, 14] is shown in Figure 1. To produce related computations, one either needs to utilize licensed commercial software (e.g., Abaqus, ANSYS, Comsol among others), dedicated open numerical software (e.g., FEniCS, FreeFEM, Netgen/NGSolve among others) or master complex knowledge of many scientific fields:

1. mathematical modeling in continuum mechanics of solids,
2. discretization of underlying (systems of) partial differential equations using FEM,
3. efficient solutions of nonlinear and linear systems of equations.

We are interested in own and complete implementations of the FEM that are understood by applied mathematicians as well as by software developers and engineers. Our implementations are reasonably documented and available for download, mostly from the MATLAB central server at <https://www.mathworks.com/matlabcentral/profile/authors/822529> .

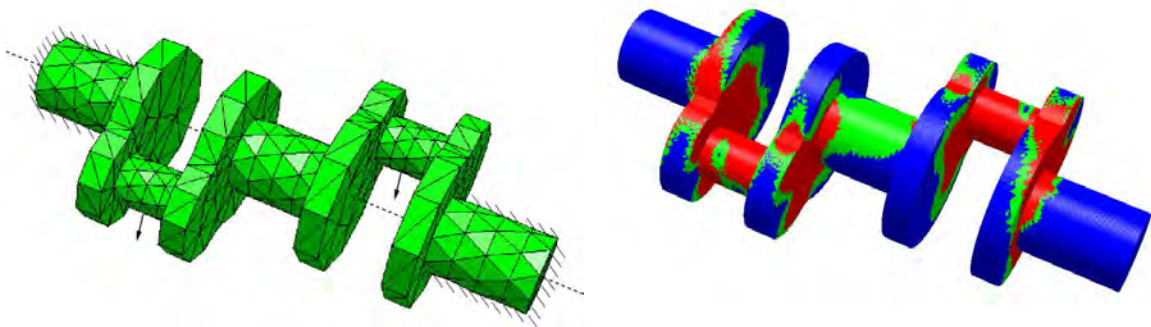


Figure 1: Crankshaft subjected to surface traction (left) and resulting elastoplastic zones (right), generated in Netgen/NGSolve software. Taken from [14].

The presented concepts provided might serve well for researchers who implement their own ideas, including students in the science, technology, engineering, and mathematics (STEM) sector who are learning practical finite element computations. Typical

mechanical engineers will be less convinced since there is no focus on particular material models or realistic physical units.

The author's Ph.D. thesis [78] of 2002 and the habilitation thesis [79] of 2011 focused on mathematical and numerical analysis of multisurface elastoplastic problems and modeling and a posteriori error estimates for some convex problems in continuum mechanics. The resulting scientific papers also included basic FEM computations without focusing on the code speed and efficiency for larger problems. It changed after the joint publications [66] with Talal Rahman (Bergen) appeared in 2013 providing vectorization tools for the FEM assemblies. Vectorization in computer science refers to performing operations all at once, instead of using loops for repeated operations. It is about replacing explicit loops with matrix and vector operations and can lead to more readable and efficient code. The publication and the attached software codes attracted the attention of non-related scientific communities in numerical computations (for instance, magnetic resonance [52] or optimal control of PDEs [34]) and led to further motivation and contributions.

Presented journal articles

This DSc. thesis is based on selected journal articles that appeared between 2013 and 2024 and are directly related or include vectorized implementations of FEM. All mentioned journal articles contain links to codes in MATLAB. The journal articles are briefly discussed in Sections 2, 3, 4.

Section 2 focuses on linear problems and consists of two journal articles. The articles dealing with nodal and edge elements in 2D and 3D provide the core of our vectorized FEM implementations. These are

- [66] RAHMAN T., VALDMAN J.: Fast MATLAB assembly of FEM matrices in 2D and 3D: nodal elements, *Applied Mathematics and Computation* **219**, No. 13, 7151–7158, 2013.
- [5] ANJAM I., VALDMAN J.: Fast MATLAB assembly of FEM matrices in 2D and 3D: edge elements, *Applied Mathematics and Computation* **267**, 252–263, 2015.

Section 3 presents three journal articles related to linearized or eigenvalue problems. The articles represent direct applications of implementations of Section 2 and [24] a modification. These are:

- [16] BOZORGNIA F., VALDMAN J.: A FEM approximation of a two-phase obstacle problem and its a posteriori error estimate, *Computers & Mathematics with Applications* **73**, No. 3, 419–432, 2017.
- [65] PAULY D., VALDMAN, J.: Friedrichs/Poincare Type Constants for Gradient, Rotation, and Divergence: Theory and Numerical Experiments, *Computers & Mathematics with Applications* **79**, No. 11, 3027–3067, 2020.
- [24] ČERMÁK M., SYSALA S., VALDMAN J.: Efficient and flexible MATLAB implementation of 2D and 3D elastoplastic problems, *Applied Mathematics and Computation* **355**, 595–614, 2019.

Finally, 4 journal articles of Section 4 deal with nonlinear problems. These are:

- [10] BEVAN J., KRUŽÍK M., VALDMAN J., Hadamard's inequality in the mean, *Nonlinear Analysis* **243**, 2024.
- [46] KRÖMER S., VALDMAN J.: Global injectivity in second-gradient Nonlinear Elasticity and its approximation with penalty terms, *Mathematics and Mechanics of Solids* **24**, No. 11, 3644–3673, 2019.

- [47] KRÖMER S., VALDMAN J.: Surface penalization of self-interpenetration in linear and nonlinear elasticity, *Applied Mathematical Modelling* **122**, 641–664, 2023.
- [57] MOSKOVKA A., VALDMAN J.: Fast MATLAB evaluation of nonlinear energies using FEM in 2D and 3D: nodal elements, *Applied Mathematics and Computation* **424**, 127048, 2022.

Each section contains a short conclusion and outlook part at its end. The remainder of this introduction contains an acknowledgment and basic mathematical notation.

Acknowledgement

I am very grateful to Prof. Martin Kružík, DSc. (Prague) for the inspiration and constant support. My colleagues Assoc. Prof. Dalibor Lukáš (Ostrava), Dr. Stanislav Sysala (Ostrava) and Dr. Tomáš Roubal (Prague) made suggestions leading to text improvements.

Notation

We denote by Ω a bounded and connected Lipschitz domain in \mathbb{R}^d , where $d \in \{2, 3\}$ denotes the dimension of the space. The domain boundary $\Gamma := \partial\Omega$ is typically divided into two segments:

- the *Dirichlet* boundary Γ_D , a closed subset of Γ with a positive surface measure,
- the *Neumann* boundary $\Gamma_N := \Gamma \setminus \Gamma_D$ (relatively open and possibly empty set).

The boundary Γ has the normal unit outward vector n . An example of a 2D domain with its boundaries is given in Figure 2.

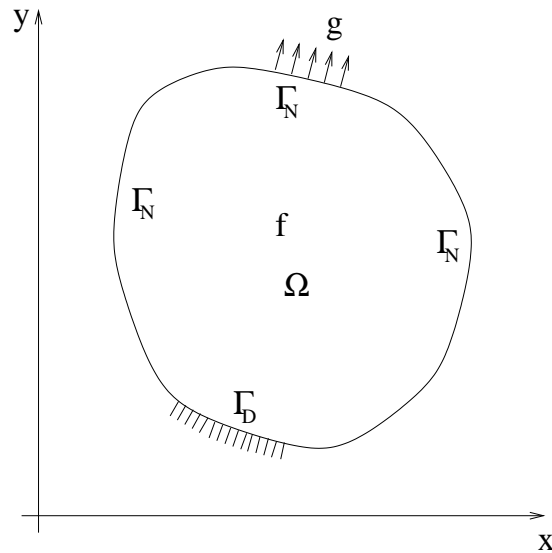


Figure 2: Material represented by the domain Ω under deformation. The material is subjected to surface forces g acting in the direction normal to the Neumann boundary Γ_N and remains intact at the Dirichlet boundary Γ_D . Taken from [78].

The concept of functional spaces is essential to formulate the models studied. The space $L^2(\Omega)$ denotes the space of integrable Lebesgue functions (with exponent 2) and the Sobolev space $H^1(\Omega)$ its subspace of Lebesgue integrable (first) weak derivatives [28].

For vector problems, these spaces naturally extend to $L^2(\Omega, \mathbb{R}^d)$ and $H^1(\Omega, \mathbb{R}^d)$. The corresponding norms are generally denoted as $\|\cdot\|$, for instance

$$\|v\|_{H^1(\Omega)} = \left(\int_{\Omega} v^2 + |\nabla v|^2 dx \right)^{1/2} \quad \forall v \in H^1(\Omega).$$

Vector problems operating with the divergence operator div and the rotation operator curl appear in electromagnetism [55] and are also related to various mixed or dual problems in mechanics. The divergence (in 2D and 3D) and rotation (in 3D) of a vector-valued function $w : \Omega \rightarrow \mathbb{R}^d$ are defined as

$$\text{div } w := \sum_{i=1}^d \partial_i w_i \quad \text{and} \quad \text{curl } w := \begin{pmatrix} \partial_2 w_3 - \partial_3 w_2 \\ \partial_3 w_1 - \partial_1 w_3 \\ \partial_1 w_2 - \partial_2 w_1 \end{pmatrix}.$$

We consider two types of rotation operators in 2D, the vector operator $\underline{\text{curl}}$ and the scalar operator curl

$$\underline{\text{curl}} f := \begin{pmatrix} \partial_2 f \\ -\partial_1 f \end{pmatrix} \quad \text{and} \quad \text{curl } w := \partial_1 w_2 - \partial_2 w_1$$

applied to a scalar function $f : \Omega \rightarrow \mathbb{R}$ and to a vector function $w : \Omega \rightarrow \mathbb{R}^2$. The operator $\underline{\text{curl}}$ is frequently called the "co-gradient" in literature, and is often denoted by ∇^\perp . The operators give rise to the standard Sobolev spaces:

$$H(\text{div}, \Omega) = \{v \in L^2(\Omega, \mathbb{R}^d) \mid \text{div } v \in L^2(\Omega)\},$$

$$H(\text{curl}, \Omega) = \begin{cases} \{v \in L^2(\Omega, \mathbb{R}^3) \mid \text{curl } v \in L^2(\Omega, \mathbb{R}^3)\} & \text{if } d = 3 \\ \{v \in L^2(\Omega, \mathbb{R}^2) \mid \text{curl } v \in L^2(\Omega)\} & \text{if } d = 2 \end{cases}.$$

Functions satisfying zero Dirichlet boundary conditions on Γ_D are denoted, for instance, as

$$H_{\Gamma_D}(\text{curl}, \Omega) = \{v \in H(\text{curl}, \Omega) \mid v \times n = 0 \text{ on } \Gamma_D\},$$

$$H_{\Gamma_D}^1(\Omega) = \{v \in H^1(\Omega)^d \mid v = 0 \text{ on } \Gamma_D\}$$

or shortly if $\Gamma = \Gamma_D$ as $H_0(\text{curl}, \Omega) = H_\Gamma(\text{curl}, \Omega)$ or $H_0^1(\Omega) = H_\Gamma^1(\Omega)$.

Assume that the domain Ω is discretized [21] by a regular triangular (2D) or a tetrahedral (3D) mesh \mathcal{T} . The elements (triangles or tetrahedra) are geometrically specified by their nodes (or vertices) that belong to the set of nodes \mathcal{N} . The nodes are also clustered on the edges of the elements (for $d \geq 2$) and the faces (for $d = 3$). We denote by \mathcal{E} the set of all edges. The numbers of nodes, edges, and elements are denoted as

$$|\mathcal{N}|, |\mathcal{E}|, |\mathcal{T}|.$$

Examples of meshes are given in Figure 3 above. Note that the left mesh consists of additionally refined triangles of the disk sector boundary, where a higher-quality numerical approximation is required. The locations of interest are predefined in this example but could be alternatively produced by an adaptive mesh refinement strategy applied to the particular type of the partial differential equation, see, e.g., [7, 18, 35].

2 Linear problems

This section is based on journal articles [5, 66]. The FEM assemblies to weak formulations of second-order elliptic partial differential equations (PDEs) are described in detail. The focus is on the lowest-order finite elements for problems formulated in gradient, curl (or rotation), and divergence differential operators. Note that divergence-related assemblies are fully documented in [5], but the explanation here follows first in Section 3 in relation to a posteriori error estimates.

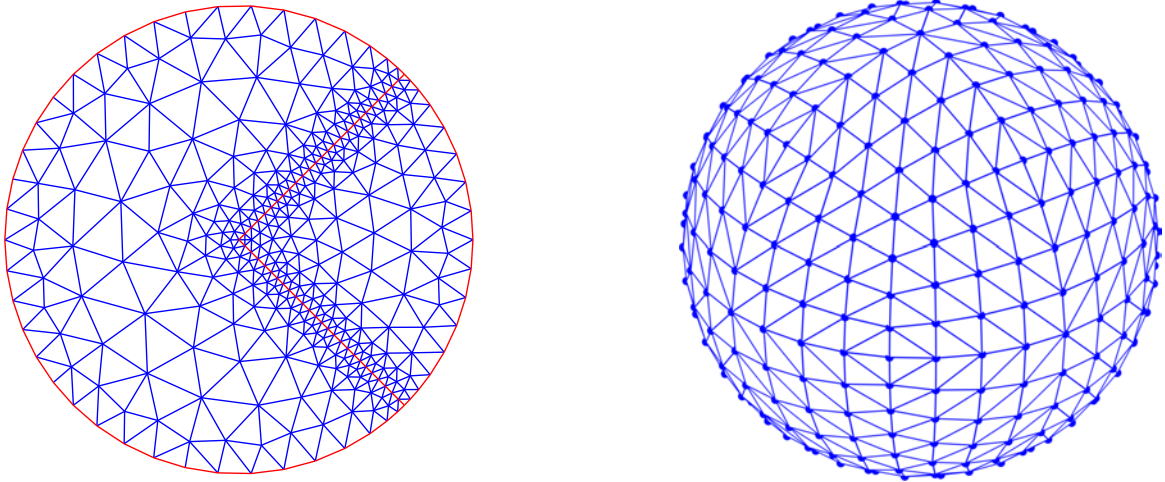


Figure 3: A triangular mesh of the disk domain (left) created by the Partial Differential Equation Toolbox of MATLAB and an own tetrahedral mesh of the sphere domain (right). Taken from [10] and [56].

2.1 Diffusion-reaction problem

A diffusion-reaction boundary value problem in one of the simplest forms reads as follows.

$$-\Delta u + \nu u = f \quad \text{in } \Omega, \quad (2.1)$$

$$\frac{\partial u}{\partial n} = 0 \quad \text{in } \partial\Omega, \quad (2.2)$$

where Δ denotes the Laplace operator and $\frac{\partial u}{\partial n}$ the derivative with respect to n and $\nu > 0$ is a parameter. The weak formulation reads

$$\int_{\Omega} \nabla u \cdot \nabla v \, dx + \nu \int_{\Omega} u v \, dx = \int_{\Omega} f v \, dx, \quad \forall v \in V, \quad (2.3)$$

where $V = H^1(\Omega)$. The approximation u_h of the solution u is searched and the test function v is chosen in the dense subset V_h of V and satisfy

$$\int_{\Omega} \nabla u_h \cdot \nabla v \, dx + \nu \int_{\Omega} u_h v \, dx = \int_{\Omega} f v \, dx, \quad \forall v \in V_h. \quad (2.4)$$

The approximation $u_h \in V_h$ is expressed as a linear combination of basis functions $\{\varphi_i\}_{i=1}^n \in V_h$ in the form

$$u_h = \sum_{i=1}^n \underline{u}_h^i \varphi_i.$$

Thus u_h is isomorphically mapped to the vector $\underline{u}_h = (\underline{u}_h^1, \dots, \underline{u}_h^n) \in \mathbb{R}^n$. The discretization of (2.4) leads to an algebraic system of linear equations

$$(\mathbf{K} + \nu \mathbf{M}) \underline{u}_h = \underline{f}_h \quad (2.5)$$

for \underline{u}_h written as a column vector. The matrices $\mathbf{K}, \mathbf{M} \in \mathbb{R}^{n \times n}$ are well-known stiffness and mass matrices with entries

$$\begin{aligned} \mathbf{K}_{ij} &= \int_{\Omega} \nabla \varphi_i \cdot \nabla \varphi_j \, dx, \\ \mathbf{M}_{ij} &= \int_{\Omega} \varphi_i \varphi_j \, dx. \end{aligned} \quad (2.6)$$

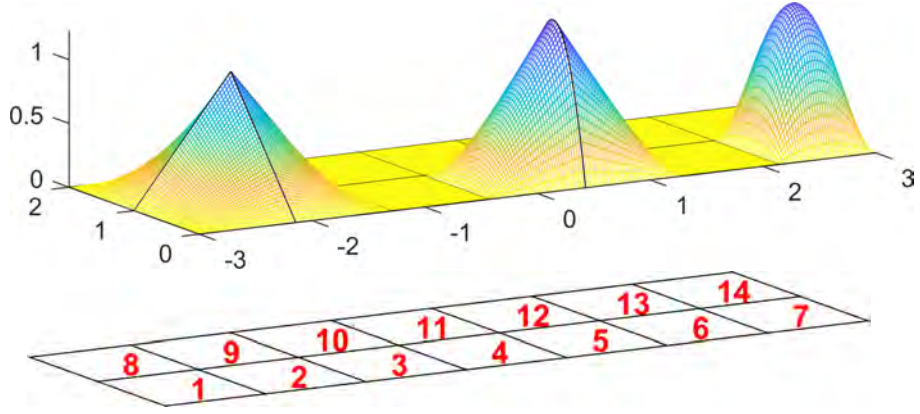


Figure 4: Example of a function $v \in S^4(\mathcal{T})$ which is composed of nodal (left), edge (middle) and bubble (right) functions. The underlying rectangular mesh with indices of elements is shown below. Taken from [58].

The vector $\underline{f}_h \in \mathbb{R}^n$ is given by $\underline{f}_h^i = \int_{\mathcal{T}} f \varphi_i dx$. The space

$$V_h = S^p(\mathcal{T}) \subset H^1(\Omega) \quad (2.7)$$

is the approximation space of p-th order polynomials on each element $T \in \mathcal{T}$ which are globally continuous functions on \mathcal{T} . It can be constructed using traditional Lagrange shape functions [21] or later developed hierarchical shape functions [74]. For illustration, an example of hierarchical basis functions on rectangles is given in Figure 4. Although we have some experience [32, 58] with higher-order hierarchical shape functions, our focus is mostly on the lowest-order polynomials, i.e., $p = 1$ or $p = 2$.

2.2 Linear elasticity

Discretization of the scalar boundary value problem explained above can be easily extended to a vector problem, such as the linear elasticity problem. The applied volume f and surface forces g shown in Figure 2 cause internal stresses within the body and are modeled by a second-order symmetric Cauchy stress tensor $\sigma : \Omega \rightarrow \mathbb{R}_{sym}^{d \times d}$. An equilibrium between external and internal forces in the quasi-static case is expressed by the equilibrium of forces

$$\operatorname{div} \sigma + f = 0 \quad \forall x \in \Omega, \quad (2.8)$$

where $f : \Omega \rightarrow \mathbb{R}^d$ denotes volumes forces (i.e., a gravity force) and $\operatorname{div} \sigma$ the divergence defined by $(\operatorname{div} \sigma)_j := \sum_{k=1}^d \frac{\partial \sigma_{jk}}{\partial x_k}$ for all $j = 1, \dots, d$. Every material point of the body moves with respect to its original position in a reference configuration Ω by a displacement $u : \Omega \rightarrow \mathbb{R}^d$. The deformation of the body is characterized for small deformations through the linearized Green strain tensor

$$\varepsilon(u) = \frac{1}{2}(\nabla u + (\nabla u)^T).$$

In linear elasticity theory we assume a linear relation between the stress σ and the deformation ε , i.e.,

$$\sigma = \mathbb{C} \varepsilon(u). \quad (2.9)$$

The linear operator $\mathbb{C} : \mathbb{R}^{d \times d} \rightarrow \mathbb{R}^{d \times d}$ denotes a symmetric, positive definite elastic tensor. For isotropic and homogeneous materials, we have that

$$\mathbb{C} \varepsilon = 2\mu \varepsilon + \lambda(\operatorname{tr} \varepsilon)\mathcal{I}, \quad (2.10)$$

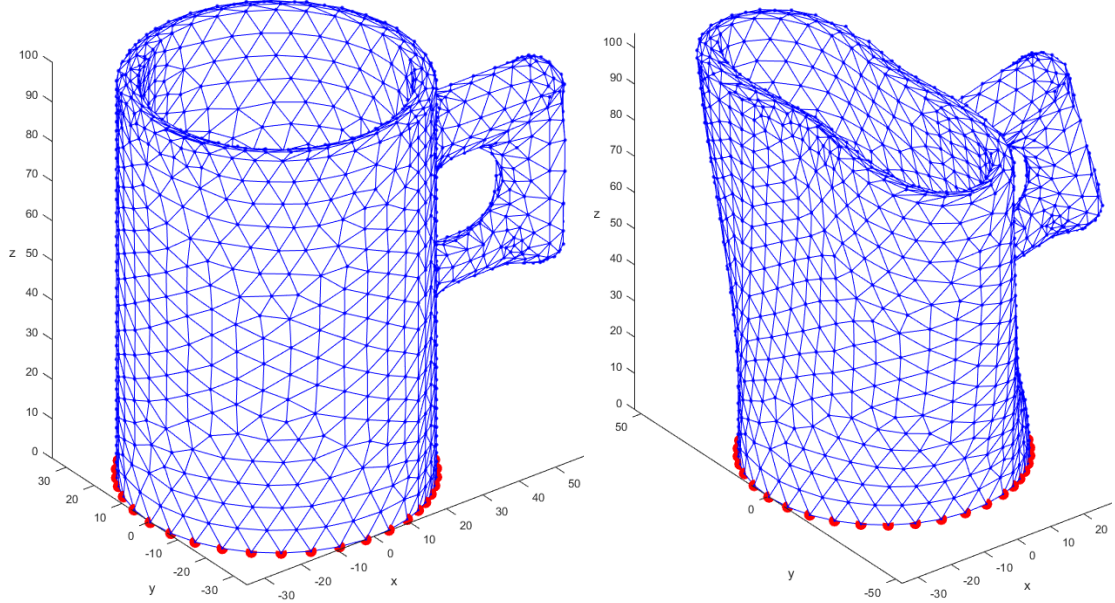


Figure 5: Elastic cup before (left) and after the deformation (right) obtained by the linear elasticity model. Taken from [42].

where the (positive) coefficients μ and λ are called Lamé coefficients. Here, \mathcal{I} denotes the second-order identity tensor (an identity matrix) and $\text{tr} : \mathbb{R}^{d \times d} \rightarrow \mathbb{R}$ defines the trace of a matrix, $\text{tr} \varepsilon := \sum_{j=1}^d \varepsilon_{jj}$, for $\varepsilon \in \mathbb{R}^{d \times d}$. We pose essential and static boundary conditions, namely $u = 0$ on Γ_D and $\sigma \cdot n = g$ on Γ_N , where g is a given applied surface force. The corresponding weak formulation reads

$$\int_{\Omega} \varepsilon(u) : \mathbb{C} \varepsilon(v) \, dx = \int_{\Omega} f \cdot v \, dx + \int_{\Gamma_N} g \cdot v \, dx \quad \forall v \in V, \quad (2.11)$$

where $V = H^1(\Omega, d)$. Here, $:$ denotes a scalar product of matrices, and it is defined as $a : b := \sum_{i,j=1}^d a_{ij} b_{ij}$. The approximation $u_h \in V_h$ of $u \in V$ is searched in the subspace $V_h \subset V$.

Remark 2.1 (for $d = 3$ only) *The vector functions $\{\eta_i\}_{i=1}^{3n} \in V_h$ of the form*

$$\begin{aligned} \eta_1 &= (\varphi_1, 0, 0), & \eta_2 &= (0, \varphi_1, 0), & \eta_3 &= (0, 0, \varphi_1), \\ \eta_4 &= (\varphi_2, 0, 0), & \eta_5 &= (0, \varphi_2, 0), & \eta_6 &= (0, 0, \varphi_2), \\ & & & \vdots & & \\ \eta_{3n-2} &= (\varphi_n, 0, 0), & \eta_{3n-1} &= (0, \varphi_n, 0), & \eta_{3n} &= (0, 0, \varphi_n) \end{aligned}$$

define one basis of V_h . Here, $\{\varphi_i\}_{i=1}^n$ are the basis functions of the scalar problem (reaction-diffusion). The reduction to $d = 2$ is obvious.

The stiffness and mass matrices $\mathbf{K}, \mathbf{M} \in \mathbb{R}^{dn \times dn}$ are given as

$$\begin{aligned} \mathbf{K}_{ij} &= \int_{\Omega} \varepsilon(\eta_i) : \mathbb{C} \varepsilon(\eta_j) \, dx, \\ \mathbf{M}_{ij} &= \int_{\Omega} \eta_i \cdot \eta_j \, dx. \end{aligned} \quad (2.12)$$

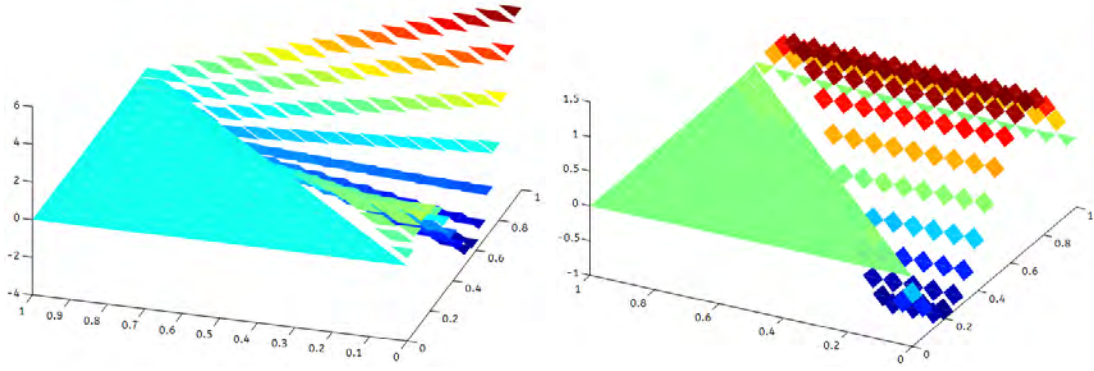


Figure 6: Components of a discrete solution $E \in H_{\Gamma_D}(\text{curl}, \Omega)$ expressed in terms of linear Nédélec shape functions. Taken from [5].

The connection of the vector and scalar basis functions of Remark 2.1 indicates that the assemblies of FEM matrices (2.12) and (2.6) are closely related.

The solution of a linear system with the stiffness matrix allows simulations of linear elasticity; see Figure 5. Linear elasticity is a simplification of the more general nonlinear theory of elasticity and a branch of continuum mechanics.

2.3 Eddy-current problem

The Maxwell equations [55] describe the interaction of electric and magnetic fields. They provide a mathematical model for electric, optical, and radio technologies, such as power generation, electric motors, wireless communication, lenses, radar, etc. They can be reduced in many ways according to their field of application. The eddy current model [45] emerges from the Maxwell equations by formally removing displacement currents (magneto-quasi-static approximation). This amounts to neglecting capacitive effects (space charges) and provides a reasonable approximation in the low-frequency range and in the presence of high conductivity. The numerical solution is possible and allows for computationally demanding approaches including coupling of FEM with the boundary element methods (BEM), preconditioning of linear systems of equations and high-order elements; see, e.g., [2, 40, 44, 72]. The simplest version of the linear magnetostatic problem reads in the (rather academic) 2D case

$$\begin{aligned}
 \underline{\text{curl}} \mu^{-1} \text{curl } E + \kappa E &= F && \text{in } \Omega, \\
 E \times n &= 0 && \text{in } \Gamma_D, \\
 \mu^{-1} \text{curl } E &= 0 && \text{in } \Gamma_N,
 \end{aligned} \tag{2.13}$$

for the vector magnetic potential $E \in H_{\Gamma_D}(\text{curl}, \Omega)$. Here, the right-hand side $F \in L^2(\Omega, \mathbb{R}^2)$, and the positive material parameters $\mu, \kappa \in L^\infty(\Omega)$ are given. If $\kappa = 0$, then the solution of the boundary value problem above is not unique and $\tilde{E} = E + \nabla\phi$ represents its solution for any function ϕ . The exact solution E is sought from the weak formulation

$$\int_{\Omega} \mu^{-1} \text{curl } E \text{ curl } w \, dx + \int_{\Omega} \kappa E \cdot w \, dx = \int_{\Omega} F \cdot w \, dx \quad \forall w \in H_{\Gamma_D}(\text{curl}, \Omega). \tag{2.14}$$

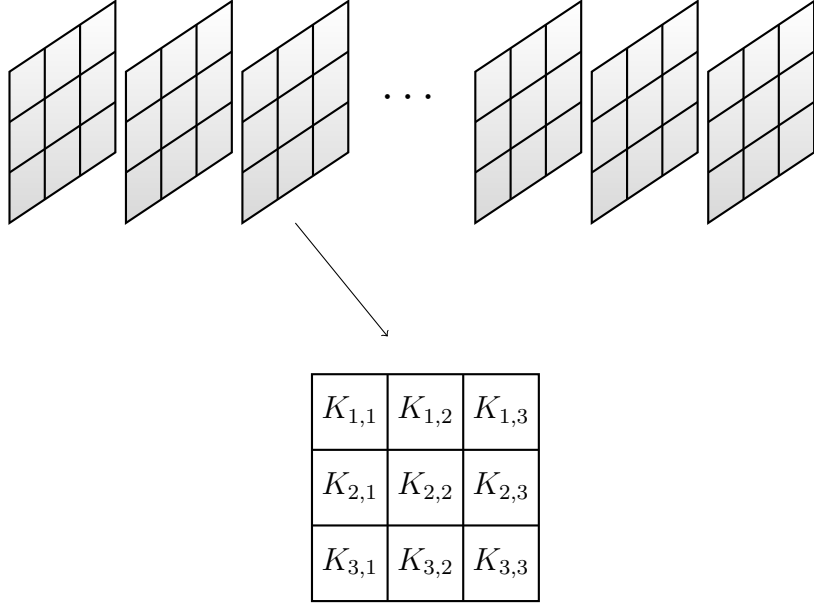


Figure 7: Local stiffness matrices are stored as slices of a tensor \mathbf{K}_{tensor} of size $3 \times 3 \times |\mathcal{T}|$.

Finite element discretization of $H_{\Gamma_D}(\text{curl}, \Omega)$ is done in terms of Nédélec shape functions [60] and utilizes the following stiffness and mass matrices

$$\begin{aligned} \mathbf{K}_{ij}^{\text{Ned}} &= \int_{\Omega} \text{curl} \eta_i^{\text{Ned}} \cdot \text{curl} \eta_j^{\text{Ned}} \, dx, \\ \mathbf{M}_{ij}^{\text{Ned}} &= \int_{\Omega} \eta_i^{\text{Ned}} \cdot \eta_j^{\text{Ned}} \, dx. \end{aligned} \quad (2.15)$$

The Nédélec shape functions (η_i^{Ned}) are not defined in the nodes of \mathcal{T} but on its edges and faces. They provide only partial continuity over the boundary of the elements: continuity of the tangential vector component for $H(\text{curl})$ problems. An example of such a function is shown in Figure 6. Vectorized assemblies of matrices (2.15) are described in [5] for the case of $d = 2, 3$.

2.4 FEM assemblies: implementation concepts

Stiffness and mass matrices are assembled from local matrices using the vectorization concepts of [5, 66] directly to [3, 4]. For illustration, we consider the case of matrices (2.6) and $d = 2$. Then, all local matrices are of size 3×3 (since there are 3 basis shape functions on a triangle) and are stored in a tensor (sometimes mentioned as a 3D array)

$$\mathbf{K}_{tensor} \in \mathbb{R}^{3 \times 3 \times |\mathcal{T}|} \quad (2.16)$$

shown schematically in Figure 7. The tensor is generated by multilinear algebra operations that are fully vectorized, so there are no loops over slices. Once the tensor is setup, it is straightforward to map it to a classical sparse stiffness matrix

$$\mathbf{K} \in \mathbb{R}^{|\mathcal{M}| \times |\mathcal{M}|}. \quad (2.17)$$

The same structure works for the local mass matrices and leads to the sparse mass matrix $\mathbf{M} \in \mathbb{R}^{|\mathcal{M}| \times |\mathcal{M}|}$. Tensor structures are fully supported in modern interpreted languages. MATLAB introduced the so-called page-wise functions in the R2020b edition. Before that, independent packages were developed, e.g., [6], among others. Vectorization leads to efficient assemblies of FEM matrices.

Example 2.2 *The assemblies for the 2D Nédélec elements and the 3D nodal elements are reported in Tables 1 and 2. The run times of both tables were obtained on*

- *the 64 Intel(R) Xeon(R) CPU E7-8837 processors running at 2.67 GHz, and 1 TB system memory (located at the University of Jyväskylä, Finland),*
- *the x4600-3.mis.mpg.de cluster with 256 Gb memory using one of 16 CPUs running on 2.8 GHz (located at MPI MIS in Leipzig, Germany).*

Both clusters were state-of-the-art clusters in the years 2015 and 2013. The run times of today's (even average scale) processors using the identical code are significantly shorter, see Table 3. An additional speed-up of the factor around 2 can be achieved by extra tuning of the underlying vectorization library, see [56].

The idea of representing the stiffness and mass matrices in a tensor format opens a new perspective that was never fully explored. Specialized versions of simple iterative methods [1] to solve systems of linear equations completely avoiding the setup of sparse matrices were reported in [53].

mesh level	size of matrices	assembly of \mathbf{K} [s]	assembly of \mathbf{M} [s]
5	9 344	0.03	0.03
6	37 120	0.11	0.47
7	147 968	0.40	1.02
8	590 848	1.82	3.65
9	2 361 344	7.49	12.94
10	9 441 280	30.83	54.86
11	37 756 928	132.56	230.44
12	151 011 328	583.86	931.79
13	604 012 544	2840.51	4121.33
14	2 415 984 640	26781.41	37009.85

Table 1: Assembly times for Nédélec elements in 2D. Taken from [5].

mesh level	size of matrices	assembly of \mathbf{K} [s]	assembly of \mathbf{M} [s]
3	15 625	1.66	0.65
4	117 649	12.49	5.73
5	912 673	105.49	48.62
6	7 189 057	1119.98	539.68

Table 2: Assembly times for nodal P^1 elements in 3D. Taken from [66].

mesh level	size of matrices	assembly of \mathbf{K} [s]	assembly of \mathbf{M} [s]
6	7 189 057	116.06	77.94

Table 3: Assembly times for nodal P^1 elements in 3D. Recomputed in 2024 on a desktop with an Intel(R) Core(TM) i7-8700 CPU @ 3.20GHz and 64 Gb memory.

Conclusion and outlooks

The articles [5, 66] represent the core of weak-form FEM assemblies that contain differential operators of gradient, rotation, or divergence type. The related codes in MATLAB are easy to read and have been downloaded by a number of users. There are altogether around 25000 reads of both articles on the ResearchGate server. However, automatic FEM assemblies have become a part of many recent mathematical codes. Thus, the value of both articles is likely to diminish, but might maintain its pedagogical value in the future.

3 Linearized and eigenvalue problems

This section is based on journal articles [5, 16, 24, 65] in which the efficient FEM assemblies of Section 2 are directly applied. We deal with

functional a posteriori estimates for the Poisson problem [5] and for the two-phase obstacle problem [16],

solvers for variational inequalities such as elastoplasticity in small strains [24] and two-phase obstacle problem [16],

eigenvalues problems [65].

3.1 A posteriori error estimate for the Poisson problem

This part contributes to functional type error a posteriori estimates developed by S. Repin, see [61] and related publications. Let us consider a scalar boundary value diffusion (Poisson's) problem

$$\begin{aligned} -\Delta u &= f && \text{in } \Omega, \\ u &= 0 && \text{on } \partial\Omega, \end{aligned}$$

for a function $u \in H_0^1(\Omega)$ and a given right hand side $f \in L^2(\Omega)$. The exact solution u is sought from the weak formulation

$$\int_{\Omega} \nabla u \cdot \nabla w \, dx = \int_{\Omega} f w \, dx \quad \forall w \in H_0^1(\Omega). \quad (3.1)$$

Assume that $v \in H_0^1(\Omega)$ is not necessarily related to any approximation of the exact solution u of (3.1). Then, the a posteriori error estimate from [61] states that

$$\|\nabla(u - v)\| \leq \|\nabla v - y\| + C_F \|\operatorname{div} y + f\| \quad \forall y \in H(\operatorname{div}, \Omega). \quad (3.2)$$

The global constant C_F represents the Friedrichs constant from the inequality

$$\|w\| \leq C_F \|\nabla w\| \quad \forall w \in H_0^1(\Omega). \quad (3.3)$$

The value of C_F is known for some academic examples or can be calculated numerically; see Subsection 3.4. Note that the estimate (3.2) is sharp: When choosing the exact flux $y = \nabla u$, the inequality changes into an equality. Since the right-hand side of (3.2)

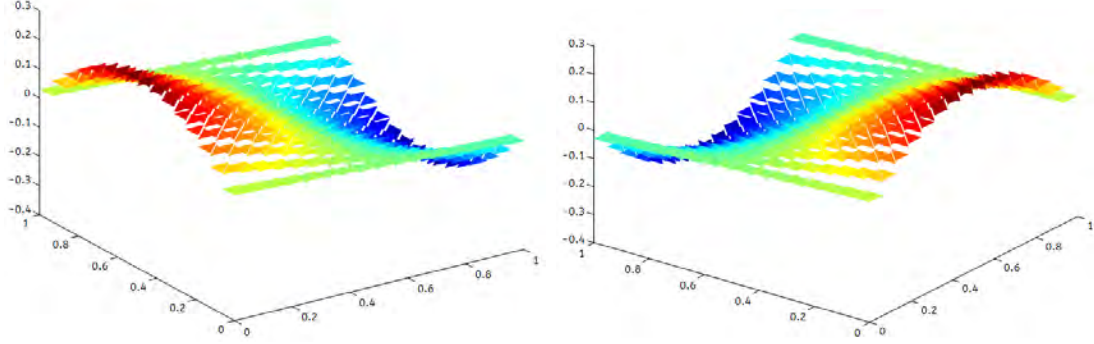


Figure 8: Components of a discrete solution $y \in H(\text{div}, \Omega)$ in terms of linear Raviart-Thomas shape functions. Taken from [5].

contains nondifferentiable norm terms, we apply Young's inequality $(a+b)^2 \leq (1+\beta)a^2 + (1+\frac{1}{\beta})b^2, \forall a, b, \beta > 0$ to obtain

$$\begin{aligned} (\|\nabla v - y\| + C_F \|\text{div} y + f\|)^2 &\leq \left(1 + \frac{1}{\beta}\right) \|\nabla v - y\|^2 + (1 + \beta) C_F^2 \|\text{div} y + f\|^2 \\ &=: \mathcal{M}(\nabla v, f, C_F, \beta, y). \end{aligned}$$

The term \mathcal{M} is called the functional error majorant. Its arguments v and f are known together with C_F . The parameter $\beta > 0$ and the function $y \in H(\text{div}, \Omega)$ are free parameters. For a fixed value of β , the majorant represents a quadratic functional in y . The global minimization of \mathcal{M} with respect to $y \in H(\text{div}, \Omega)$ results in the following weak formulation:

$$\begin{aligned} (1 + \beta) C_F^2 \int_{\Omega} \text{div} y \text{div} \phi \, dx + \left(1 + \frac{1}{\beta}\right) \int_{\Omega} y \cdot \phi \, dx \\ = -(1 + \beta) C_F^2 \int_{\Omega} f \text{div} \phi \, dx + \left(1 + \frac{1}{\beta}\right) \int_{\Omega} \nabla v \cdot \phi \, dx \end{aligned} \quad (3.4)$$

valid for $\forall \phi \in H(\text{div}, \Omega)$. On the other hand, for a fixed y ,

$$\beta = \frac{\|\nabla v - y\|}{C_F \|\text{div} y + f\|} \quad (3.5)$$

minimizes \mathcal{M} amongst all $\beta > 0$. The discretization of the left side of (3.4) requires the assembly of stiffness and mass matrices

$$\begin{aligned} \mathbf{K}_{ij}^{\text{RT}} &= \int_{\Omega} \text{div} \eta_i^{\text{RT}} \text{div} \eta_j^{\text{RT}} \, dx, \\ \mathbf{M}_{ij}^{\text{RT}} &= \int_{\Omega} \eta_i^{\text{RT}} \cdot \eta_j^{\text{RT}} \, dx, \end{aligned} \quad (3.6)$$

where the Raviart-Thomas shape functions (η_i^{RT}) are used, cf. [67]. They are (similarly to the Nédélec shape functions explained in Subsection 2.3) not defined on the nodes of but on the edges and faces. They also provide only partial continuity over element boundaries: continuity of the normal vector component for $H(\text{div})$ problems. An example of such a function is shown in Figure 8.

The solution of the corresponding linear systems of equation in terms of the multigrid preconditioned conjugate gradient method is explained in [76].

3.2 A posteriori error estimate for the two-phase obstacle problem

This part is based on [16]. A general form of elliptic free boundary problems can be written as

$$\Delta u = f(x, u, \nabla u) \quad \text{in } \Omega, \quad (3.7)$$

where the right-hand side term is piecewise continuous, having jumps at some values of the arguments u and ∇u . We are concerned about the particular elliptic free boundary problem

$$\Delta u = \alpha_+ \chi_{\{u>0\}} - \alpha_- \chi_{\{u<0\}} \quad \text{in } \Omega, \quad (3.8)$$

$$u = g \quad \text{on } \partial\Omega. \quad (3.9)$$

Here, χ_A denotes the characteristic function of the set A , $\alpha_{\pm} : \Omega \rightarrow \mathbb{R}$ are positive and Lipschitz continuous functions and $g \in W^{1,2}(\Omega) \cap L^{\infty}(\Omega)$ and g changes sign on $\partial\Omega$.

Remark 3.1 *The problem (3.8) describes a complete reaction of two substances coming into contact with an elastic membrane, and is sometimes referred to as the “two-phase membrane” problem. If the densities of the substances are given as ρ_1 and ρ_2 and the elastic membrane has the density ρ_m that satisfies*

$$\rho_1 > \rho_m > \rho_2,$$

then α_+ is proportional to the difference $\rho_1 - \rho_m$ and α_- is proportional to the difference $\rho_m - \rho_2$. Note that if we let $\alpha^- = 0$, and assume that g is nonnegative on the boundary, then we obtain the well-known one-phase obstacle problem; see, e.g., [17, 43].

The set

$$(\partial\{x \in \Omega : u(x) > 0\} \cup \partial\{x \in \Omega : u(x) < 0\}) \cap \Omega$$

is called the free boundary. The properties of the solution of the two-phase obstacle problem, the regularity of the solution, and the free boundary have been studied, for example, in [73]. It is known that (3.8)-(3.9) represents the Euler-Lagrange equation corresponding to the minimizer of the energy functional

$$J(v) = \int_{\Omega} \left(\frac{1}{2} |\nabla v|^2 + \alpha_+ v^+ + \alpha_- v^- \right) dx \quad (3.10)$$

over the affine space $K = \{v \in H^1(\Omega) : v - g \in H_0^1(\Omega)\}$. Here, $v^+ = \max(v, 0)$ and $v^- = \max(-v, 0)$ denote the (point-wise) positive and negative parts of v . The functional $J : K \rightarrow \mathbb{R}$ is convex, coercive on K and weakly lower semi-continuous, hence the unique minimum of J is attained at some $u \in K$. An example of calculating u for a benchmark with only partial Dirichlet conditions (see [16] for details) is shown in Figure 9. Using a perturbed functional and an inf-sup condition we can reformulate the minimization of $J(v)$ as a maximization of the corresponding dual functional expressed for a multiplier $\mu \in \Lambda$ the space

$$\Lambda := \{\mu \in L^{\infty}(\Omega) : \mu(x) \in [-\alpha_-, \alpha_+] \text{ a.e. in } \Omega\}.$$

By exploiting dual conjugate and compound functionals it is possible to derive so-called *energy identities* and further estimate them from above [16] in terms of *the majorant estimate*

$$J(v) - J(u) \leq M_+(v; \beta, y, \mu) \quad \forall v \in K, \mu \in \Lambda, y \in H(\Omega, \text{div}), \beta > 0. \quad (3.11)$$

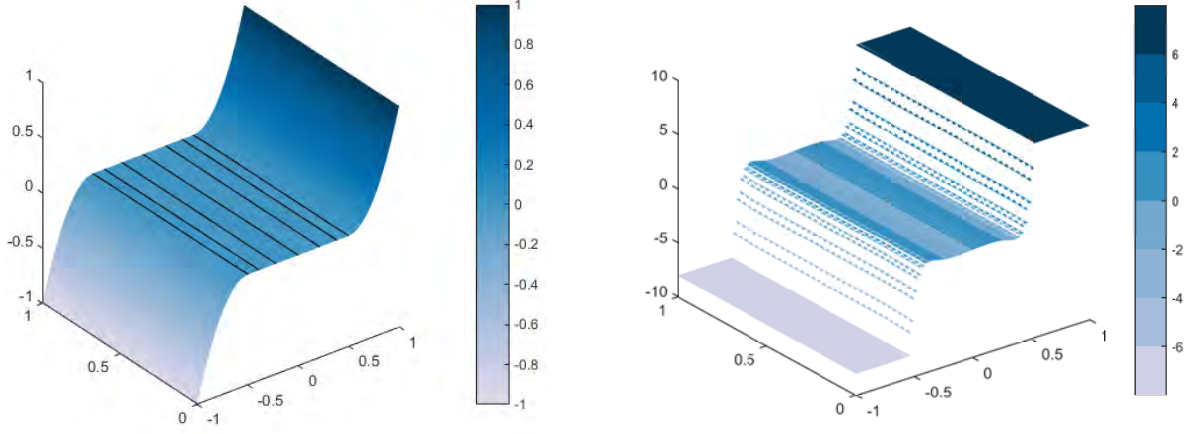


Figure 9: Approximation of $u_h \in K$ with the full contour lines at values ± 0.0001 (left) and of the corresponding Lagrange multiplier $\lambda_h \in \Lambda$ (right). The multiplier indicates an approximate free boundary while the lines $x = \pm 0.5$ give the exact free boundary. Taken from [16].

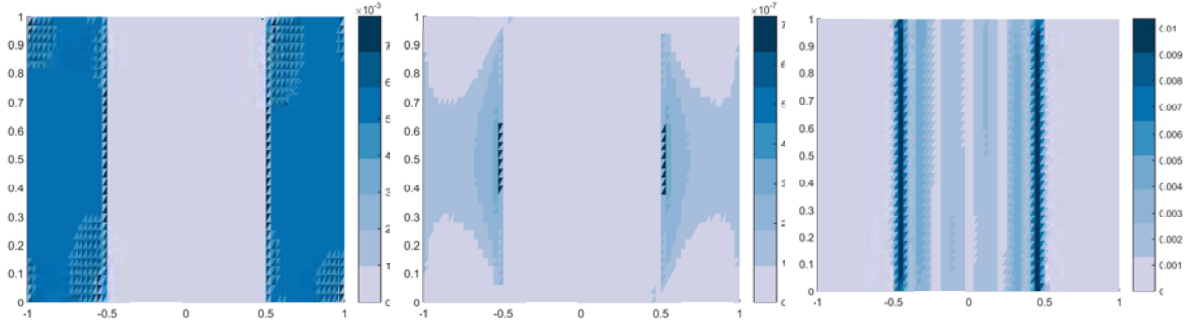


Figure 10: Distribution of the majorant parts: the gradient part \mathcal{M}_{+1} (left), the equilibrium part \mathcal{M}_{+2} (middle), the nonlinear part \mathcal{M}_{+3} (right) corresponding to $v = u_h$ and $\mu = \lambda_h$ of Figure 9 and optimized β and y . Taken from [16].

The nonnegative functional

$$M_+(v; \beta, y, \mu) = \mathcal{M}_{+1}(v; \beta, y) + \mathcal{M}_{+2}(\beta, y, \mu) + \mathcal{M}_{+3}(v; \mu) \quad (3.12)$$

represents a functional error majorant and consists of three additive parts

$$\begin{aligned} \mathcal{M}_{+1}(v; \beta, y) &= \frac{1}{2}(1 + \beta) \|\nabla v - y\|_{L^2(\Omega)}^2, \\ \mathcal{M}_{+2}(\beta, y, \mu) &= \frac{1}{2}\left(1 + \frac{1}{\beta}\right) C_F^2 \|\operatorname{div} y - \mu\|_{L^2(\Omega)}^2, \\ \mathcal{M}_{+3}(v; \mu) &= \int_{\Omega} \left(\alpha_+ v^+ + \alpha_- v^- - \mu v \right) dx. \end{aligned} \quad (3.13)$$

All above majorant parts are fully computable and their densities indicate locations of the error of approximation $v \in K$, see Figure 10. The left part indicates the error in the gradient, the middle part the error in the equilibrium, and the right part the error in the nonlinear relation.

We recall the occurrence of

- the matrices \mathbf{K}, \mathbf{M} from (2.6) at the calculation of $v \in K$,
- the matrices $\mathbf{K}^{\text{RT}}, \mathbf{M}^{\text{RT}}$ from (3.6) at the calculation of $y \in H(\Omega, \operatorname{div})$.

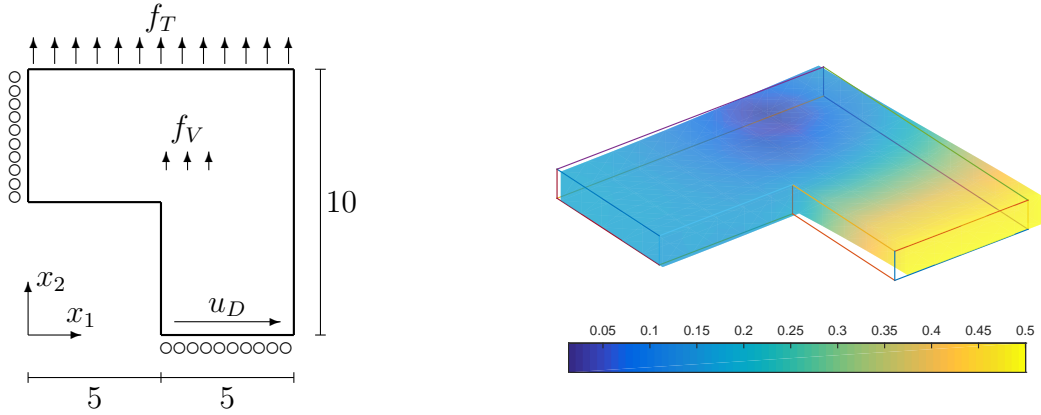


Figure 11: Simplified 2D geometry of the elastic problem (left). The real 3D geometry appears by extrusion in the x_3 direction. The corresponding total displacement field $\|u\|$ is displayed in a deformed configuration (right). Taken from [24].

3.3 Elastoplasticity in small strains

Elastoplastic problems represent an important topic in the nonlinear continuum mechanics of solids. They are characterized as time-dependent (quasi-static) problems that involve models with various yield criteria, flow rules, or internal variables [39, 64]. The model of additive plasticity assumes a linear relation

$$\sigma = \mathbb{C}(\varepsilon(u) - p), \quad (3.14)$$

where the additional plastic strain p is represented by a symmetric and trace-free tensor. The evolution of plastic strain is subject to the above-mentioned flow rules. Elastoplasticity can be described as a parabolic (in time) second kind variational inequality [39]. A standard computational procedure consisting of the following steps [75]:

- (a) implicit time-discretization of a constitutive initial-value problem,
- (b) construction of a constitutive operator and its generalized derivative,
- (c) space discretization by the finite element method,
- (d) solution of a resulting discretized system by the (semismooth) Newton method.

Figure 11 shows an example of an elastoplastic benchmark. The corresponding time-discretized elastoplastic problem is formulated in terms of displacement u , in each time step we solve a system of nonlinear equations of the following type:

$$\text{find } \underline{u}_h \in \mathbb{R}^n : \quad F(\underline{u}_h) = \underline{f}_h, \quad (3.15)$$

where \underline{u}_h denotes the unknown displacement vector, $\underline{f}_h \in \mathbb{R}^n$ is the vector of external forces, and $F: \mathbb{R}^n \rightarrow \mathbb{R}^n$ is a nonlinear function representing internal forces which is usually Lipschitz continuous and semismooth but nonsmooth in \mathbb{R}^n . Therefore, it is necessary to use the semismooth variant of the Newton method, see [36]. In each Newton iteration $\ell = 0, 1, 2, \dots$, we solve a linear system of equations of the following type:

$$\text{find } \delta \underline{u}_h^\ell \in \mathbb{R}^n : \mathbf{K}_{\text{tangent}} \delta \underline{u}_h^\ell = \underline{f}_h - F(\underline{u}_h^\ell), \quad (3.16)$$

where $\delta \underline{u}_h^\ell \in \mathbb{R}^n$ is an unknown incremental vector, $\underline{u}_h^\ell \in \mathbb{R}^n$ is a previous iteration of \underline{u}_h , and $\mathbf{K}_{\text{tangent}} \in \mathbb{R}^{n \times n}$ is a tangential stiffness matrix representing a generalized derivative

of F at $\underline{u}_h^\ell \in \mathbb{R}^n$. The tangential matrix changes in every iteration, but can be efficiently assembled in the form

$$\mathbf{K}_{\text{tangential}} = \mathbf{K}_{\text{elastic}} + \mathbf{B}^\top (\mathbf{D}_{\text{tangential}} - \mathbf{D}_{\text{elastic}}) \mathbf{B}, \quad (3.17)$$

where \mathbf{B} is a sparse matrix representing the strain-displacement operator at all integration points, $\mathbf{D}_{\text{tangential}}$, $\mathbf{D}_{\text{elastic}}$ are block diagonal sparse matrices for elastic and elastoplastic problems and

$$\mathbf{K}_{\text{elastic}} = \mathbf{B}^\top \mathbf{D}_{\text{elastic}} \mathbf{B}. \quad (3.18)$$

Each block of $\mathbf{D}_{\text{tangential}}$, $\mathbf{D}_{\text{elastic}}$ is represented by the derivative of constitutive operators. The matrices $\mathbf{K}_{\text{elastic}}$, \mathbf{B} , $\mathbf{D}_{\text{elastic}}$ can be precomputed, and only matrix $\mathbf{D}_{\text{tangential}}$ depends on a particular plasticity model and needs to be partially reassembled in each Newton iteration. For problems with smaller plastic regions, the assembly of the tangential stiffness matrix can be significantly faster than for problems with larger plastic regions.

Remark 3.2 *The techniques described above are explained in [24]. The implementation of the decomposition (3.18) is fully competitive with assemblies of [66].*

3.4 Eigenvalue problems

Eigenvalue problems are highly relevant for many applications. Typical examples are, e.g., structural vibrations, material science, electromagnetic, and acoustic waves. Their combination with the finite element method [15] provides approximate eigenvalues and the corresponding eigenfunctions. Assume Ω is a bounded Lipschitz domain in \mathbb{R}^d . The smallest constants $c_{n,\Gamma} > 0$ for $n = 0, 1, 2$ arising in estimates of the form

$$\|u\|_{\mathbf{L}^2(\Omega)} \leq c_{0,\Gamma} \|\text{grad } u\|_{\mathbf{L}^2(\Omega)} \quad \forall v \in H_0^1(\Omega), \quad (3.19)$$

$$\|E\|_{\mathbf{L}^2(\Omega)} \leq c_{1,\Gamma} \|\text{curl } E\|_{\mathbf{L}^2(\Omega)} \quad \forall E \in H_0(\text{curl}, \Omega) \cap H_0(\text{curl} = 0, \Omega)^\perp, \quad (3.20)$$

$$\|H\|_{\mathbf{L}^2(\Omega)} \leq c_{2,\Gamma} \|\text{div } H\|_{\mathbf{L}^2(\Omega)} \quad \forall H \in H_0(\text{div}, \Omega) \cap H_0(\text{div} = 0, \Omega)^\perp \quad (3.21)$$

play a crucial role in the analysis of elliptic boundary value problems with Dirichlet boundary conditions on Γ . Similarly, the smallest constants $c_{n,\emptyset} > 0$ for $n = 0, 1, 2$ in estimates

$$\|u\|_{\mathbf{L}^2(\Omega)} \leq c_{0,\emptyset} \|\text{grad } u\|_{\mathbf{L}^2(\Omega)} \quad \forall v \in H^1(\Omega) \cap \mathbb{R}^\perp, \quad (3.22)$$

$$\|E\|_{\mathbf{L}^2(\Omega)} \leq c_{1,\emptyset} \|\text{curl } E\|_{\mathbf{L}^2(\Omega)} \quad \forall E \in H(\text{curl}, \Omega) \cap H(\text{curl} = 0, \Omega)^\perp, \quad (3.23)$$

$$\|H\|_{\mathbf{L}^2(\Omega)} \leq c_{2,\emptyset} \|\text{div } H\|_{\mathbf{L}^2(\Omega)} \quad \forall H \in H(\text{div}, \Omega) \cap H(\text{div} = 0, \Omega)^\perp \quad (3.24)$$

are met in the analysis of elliptic boundary value problems with Neumann boundary conditions on Γ . The constants are known, in general, as Laplace and Maxwell constants. Their values are also directly entered into a posteriori error estimates and can be approximated numerically from above in the corresponding FEM spaces (\mathbf{P}^1 , Ned, RT) as

$$c_{0,\Gamma,\mathbf{P}^1}, \quad c_{1,\Gamma,\text{Ned}}, \quad c_{2,\Gamma,\text{RT}}, \quad c_{0,\emptyset,\mathbf{P}^1}, \quad c_{1,\emptyset,\text{Ned}}, \quad c_{2,\emptyset,\text{RT}}.$$

For instance, the classical Friedrichs constant $c_{0,\Gamma}$ is approximated as

$$\frac{1}{c_{0,\Gamma,\mathbf{P}^1}^2} = \lambda_{0,\Gamma,\mathbf{P}^1}^2 = \min_{\substack{0 \neq \underline{u}^{\mathbf{P}^1} \\ \underline{u}_\Gamma^{\mathbf{P}^1} = 0}} \frac{\mathbf{K}^{\mathbf{P}^1} \underline{u}^{\mathbf{P}^1} \cdot \underline{u}^{\mathbf{P}^1}}{\mathbf{M}^{\mathbf{P}^1} \underline{u}^{\mathbf{P}^1} \cdot \underline{u}^{\mathbf{P}^1}}, \quad (3.25)$$

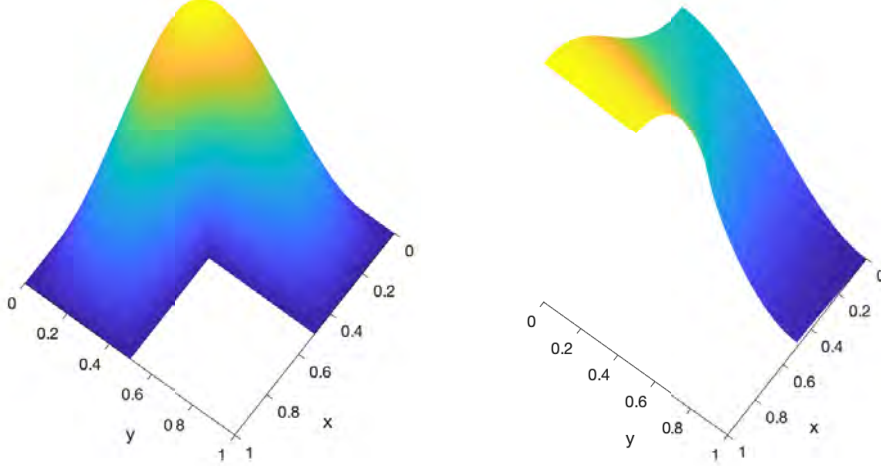


Figure 12: Eigenfunctions from the Friedrichs (left) and Poincaré (right) inequalities for the L-shape domain. Taken from [65].

where $\underline{u}_\Gamma^{\text{P}^1}$ denotes a subvector of the vector $\underline{u}^{\text{P}^1}$ in indices corresponding to boundary nodes. The constant $\lambda_{0,\Gamma,\text{P}^1}^2$ represents the minimal Rayleigh quotient of the quadratic forms above, and it is therefore equal to the minimal (positive) eigenvalue of the generalized eigenvalue problem

$$\mathbf{K}^{\text{P}^1} \underline{u}^{\text{P}^1} = \lambda^2 \mathbf{M}^{\text{P}^1} \underline{u}^{\text{P}^1}, \quad \underline{u}_\Gamma^{\text{P}^1} = 0, \quad (3.26)$$

where \mathbf{K}^{P^1} and \mathbf{M}^{P^1} are stiffness and mass matrices identical to (2.6). Alternatively, it may be found by computing the minimal (positive) eigenvalue of

$$\mathbf{K}_{\text{int}}^{\text{P}^1} \underline{u}_{\text{int}}^{\text{P}^1} = \lambda^2 \mathbf{M}_{\text{int}}^{\text{P}^1} \underline{u}_{\text{int}}^{\text{P}^1}, \quad (3.27)$$

where $\mathbf{K}_{\text{int}}^{\text{P}^1}$, $\mathbf{M}_{\text{int}}^{\text{P}^1}$, and $\underline{u}_{\text{int}}^{\text{P}^1}$ are restrictions of the matrices \mathbf{K}^{P^1} , \mathbf{M}^{P^1} , and the vector $\underline{u}^{\text{P}^1}$, respectively, to indices corresponding to internal mesh nodes only. Note that $\mathbf{K}_{\text{int}}^{\text{P}^1}$ is regular.

The classical Poincaré constant $c_{0,\emptyset}$ is approximated as

$$\frac{1}{c_{0,\emptyset,\text{P}^1}^2} = \lambda_{0,\emptyset,\text{P}^1}^2 = \min_{\substack{0 \neq \underline{u}^{\text{P}^1} \\ \underline{u}^{\text{P}^1} \cdot \mathbf{1}^{\text{P}^1} = 0}} \frac{\mathbf{K}^{\text{P}^1} \underline{u}^{\text{P}^1} \cdot \underline{u}^{\text{P}^1}}{\mathbf{M}^{\text{P}^1} \underline{u}^{\text{P}^1} \cdot \underline{u}^{\text{P}^1}}, \quad (3.28)$$

where the constraint $\underline{u}^{\text{P}^1} \cdot \mathbf{1}^{\text{P}^1} = 0$ means that the vector $\underline{u}^{\text{P}^1}$ has to be perpendicular to the constant vector of ones. The value $\lambda_{0,\emptyset,\text{P}^1}^2$ is the minimal positive eigenvalue of the generalized eigenvalue problem

$$\mathbf{K}^{\text{P}^1} \underline{u}^{\text{P}^1} = \lambda^2 \mathbf{M}^{\text{P}^1} \underline{u}^{\text{P}^1}. \quad (3.29)$$

The minimal eigenvalue here is $\lambda^2 = 0$ and the corresponding eigenvector is the constant vector of ones. Similar generalized eigenvalue problems with stiffness and mass matrices \mathbf{K}^{Ned} , \mathbf{M}^{Ned} given by (2.15) or \mathbf{K}^{RT} , \mathbf{M}^{RT} given by (3.6) can be treated. The results of the computation for the L-shape domain are summarized in Table 4 and two corresponding eigenfunctions are visualized in Figure 12. We notice that all approximate values accumulate to two possible values. It is not a coincidence, since it holds

$$c_{0,\emptyset} = c_{2,\Gamma} = c_{1,\Gamma}, \quad c_{1,\emptyset} = c_{2,\emptyset} = c_{0,\Gamma}, \quad (3.30)$$

mesh level	c_{0,\emptyset,P^1}	$c_{2,\Gamma,RT}$	$c_{1,\Gamma,Ned}$	$c_{1,\emptyset,Ned}$	$c_{2,\emptyset,RT}$	c_{0,Γ,P^1}
1	0.39156654	0.43611331	0.43611331	0.16795692	0.16795692	0.13325394
2	0.40370423	0.42045050	0.42045050	0.16377267	0.16377267	0.15232573
3	0.40850306	0.41492017	0.41492017	0.16214127	0.16214127	0.15838355
4	0.41038725	0.41287500	0.41287500	0.16148392	0.16148392	0.16020361
5	0.41112643	0.41209870	0.41209870	0.16121879	0.16121879	0.16076463
6	0.41141712	0.41179918	0.41179918	0.16111230	0.16111230	0.16094566
7	0.41153175	0.41168242	0.41168242	0.16106970	0.16106970	0.16100698

Table 4: Constants approximations computed for the L-shape domain. Taken from [65].

but this result only applies to the dimension $d = 2$. See [65] for an extension to $d = 3$ and a mixture of boundary conditions.

Conclusion and outlooks

The outputs of Section 2 are utilized in journal articles [5, 16, 24, 65] presented in this Section 3. The articles were completed in collaboration with different scientific communities with different aims: to push vectorized implementations even further into a new field or to support new theoretical concepts computationally. More contributions would also fall within this section, but were not included because of the absence of vectorized FEM techniques or rather technical details, e.g., from variational analysis. These are

scalar and elasticity problems with nonlinear boundary conditions [62, 68],

scalar problems with obstacles and their error identities [69],

static elasticity contact problems with Coulomb friction and their semismooth* Newton solvers [37].

In terms of reader popularity, the most downloaded article is [24] with around 4500 reads on the ResearchGate server. The reason might be that the corresponding MATLAB code is clearly documented and ready to use. We are also currently testing it with colleagues from the Institute of Thermomechanics of the CAS for 3D simulations of shape-memory alloys.

4 Nonlinear problems

This section consists of journal articles [10, 46, 47, 57]. The first three articles are based on collaborations with colleagues in the theoretical field of calculus of variations. We recall that efficient implementations of FEM also serve as an important tool for the verification and illustration of the theoretical results of the attached papers. The last article provides a new approach to automatically minimizing nonlinear energetic formulations.

4.1 Hadamard inequality in mean

Assume that $\Omega \subset \mathbb{R}^2$ and consider $y : \Omega \rightarrow \mathbb{R}^2$ such that the boundary value $y(x) = y_0(x)$ is given on $\partial\Omega$. We want to show that the quadratic energy

$$F(y) = \int_{\Omega} |\nabla y|^2 + f(x) \det \nabla y \, dx \quad (4.1)$$

is minimized by $\psi \in W^{1,2}(\Omega; \mathbb{R}^2)$ such that $\psi = y_0$ on the boundary. The energy is frame invariant, that is, $F(y) = F(Qy)$ holds for all rotation matrices $Q \in SO(2)$. Writing $y(x) = \psi(x) + \varphi(x)$, where $\varphi(x) = 0$ for $x \in \partial\Omega$ leads to matrix equalities

$$\begin{aligned} |\nabla y|^2 &= |\nabla\psi + \nabla\varphi|^2 = |\nabla\psi|^2 + 2\nabla\psi : \nabla\varphi + |\nabla\varphi|^2, \\ \det\nabla y &= \det(\nabla\psi + \nabla\varphi) = \det\nabla\psi + \operatorname{cof}\nabla\psi : \nabla\varphi + \det\nabla\varphi, \end{aligned}$$

where \det and cof denote the determinant and cofactor matrix operators. Hence,

$$F(y) - F(\psi) = I_2(\varphi, f) + \int_{\Omega} 2\nabla\psi : \nabla\varphi + f \operatorname{cof}\nabla\psi : \nabla\varphi \, dx, \quad (4.2)$$

where

$$I_2(\varphi, f) := \int_{\Omega} |\nabla\varphi|^2 + f(x) \det\nabla\varphi \, dx \quad \varphi \in W_0^{1,2}(\Omega, \mathbb{R}^2). \quad (4.3)$$

Thus, F is convex if and only if $I_2(\varphi, f) \geq 0$ for all $\varphi \in W_0^{1,2}(\Omega, \mathbb{R}^2)$. On the other hand, as ψ is a minimizer

$$\int_{\Omega} 2\nabla\psi : \nabla\varphi + f \operatorname{cof}\nabla\psi : \nabla\varphi \, dx = 0 \quad (4.4)$$

if ψ is a stationary point of F , see [10, Prop. 2.1 (ii)]. Hence, ψ is a minimizer of F if and only if $I_2(\varphi, f) \geq 0$. In particular, if F has two minimizers then the set of minimizers is unbounded in $W^{1,2}(\Omega; \mathbb{R}^2)$ and F has infinitely many minimizers. More generally, the paper [10] concerns the functional

$$I_n(\varphi, f) = \int_{\Omega} |\nabla\varphi|^n + f \det\nabla\varphi \, dx \quad \varphi \in W_0^{1,n}(\Omega; \mathbb{R}^n) \quad (4.5)$$

for $n \geq 2$ and a Lipschitz domain Ω in \mathbb{R}^n and $f \in L^\infty(Q)$.

Remark 4.1 *The classical pointwise Hadamard inequality is*

$$|A|^n \geq c_n |\det A|, \quad \forall A \in \mathbb{R}^{n \times n}, \quad (4.6)$$

where $|A|^2 = \sum_{i,j=1}^n A_{ij}^2$ represents the Frobenius norm of the square matrix A . The largest positive constant c_n that satisfies the inequality is $c_n = n^{\frac{n}{2}}$, which is proved by the use of the arithmetic-geometric mean inequality. Consequently, the pointwise inequality

$$|A|^n + c \det A \geq 0, \quad \forall A \in \mathbb{R}^{n \times n} \quad (4.7)$$

will be violated for any $c > c_n$.

By a Hadamard-in-the-mean inequality, henceforth (HIM), we mean an inequality

$$I_n(\varphi, f) \geq 0 \quad \forall \varphi \in W_0^{1,n}(\Omega, \mathbb{R}^n). \quad (\text{HIM})$$

The inequality (HIM) can be seen as a nonlocal version of the Morrey quasi-convexity condition [25], which means that f is a constant function. Indeed, in this case, the integrand is quasi-convex. The fact that (HIM) holds for more general f is already indicated by the observation that

$$\int_{\Omega} \det\nabla\varphi \, dx = 0 \quad \forall \varphi \in W_0^{1,n}(\Omega, \mathbb{R}^n) \quad (4.8)$$

0	$-\sqrt{8}$
$+\sqrt{8}$	0

Figure 13: Distribution of f yielding $I_2(\varphi) \geq 0$ for any $\varphi \in W_0^{1,2}(\Omega; \mathbb{R}^2)$. Taken from [10].

because the map $\mathbb{R}^{n \times n} \rightarrow \mathbb{R}: F \mapsto \det F$ is a so-called null Lagrangian; cf. e.g., [25]. Hence, if f is a constant function of any magnitude, then (HIM) always holds.

However, if f is nonconstant, the problem is much more difficult. We analyzed it in a few special cases in [10], however, a general case is out of reach. Interestingly, although the integrand is nonconvex the functional might be convex in some cases, c.f. [11]. We can find that (HIM) holds for those essentially bounded and measurable functions f that obey

$$\|f - \bar{f}_\Omega\|_\infty \leq n^{\frac{n}{2}}, \quad (4.9)$$

where $\bar{f}_\Omega = \int_\Omega f dx$ denotes the average of f in the domain Ω . In particular examples, the actual jump of f can be even higher; see Figure 13. This example of [10] is optimal in the sense that if the f -values $\pm\sqrt{8}$ are replaced by $\pm(\sqrt{8} + \epsilon)$ for any positive ϵ then there are $\varphi \in W_0^{1,2}(\Omega; \mathbb{R}^2)$ such that $I_2(\varphi) < 0$. Calculating the optimal distribution of f is complicated but possible, using the harmonicity of the minimizer in four quarters.

A verification tool and an alternative to analytical computations is a numerical implementation that uses the finite element method. The function f is assumed to be a piecewise constant in smaller subdomains. If the triangulation is aligned with subdomain shapes, then the numerical quadrature of both terms in (4.5) is exact. Based on the initial guess provided, the trust-region method aims to find the minimizer $\varphi = (\varphi_1, \varphi_2)$. If an argument is found for which the energy value drops below a negative prescribed value, the computation ends with the result that the problem is unbounded; see Figure 14. Otherwise, the problem is bounded and the minimum energy equals zero.

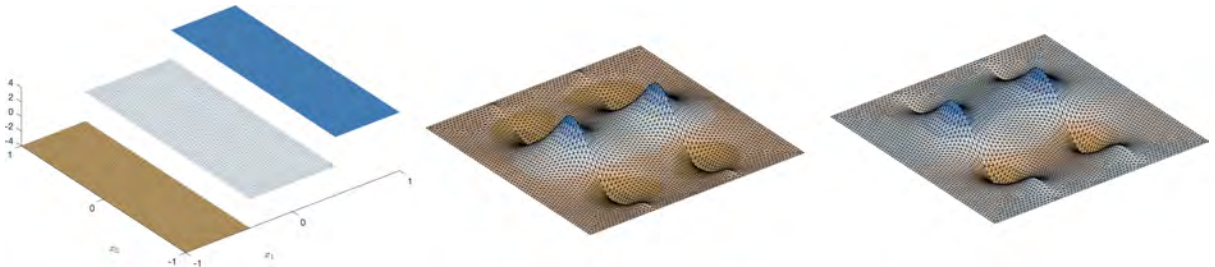


Figure 14: Insulation problem: distribution of f (left), components φ_1 (middle), and φ_2 (right) of the corresponding minimizer $\varphi = (\varphi_1, \varphi_2)$ providing $I_2(\varphi, f) < 0$. Taken from [10].

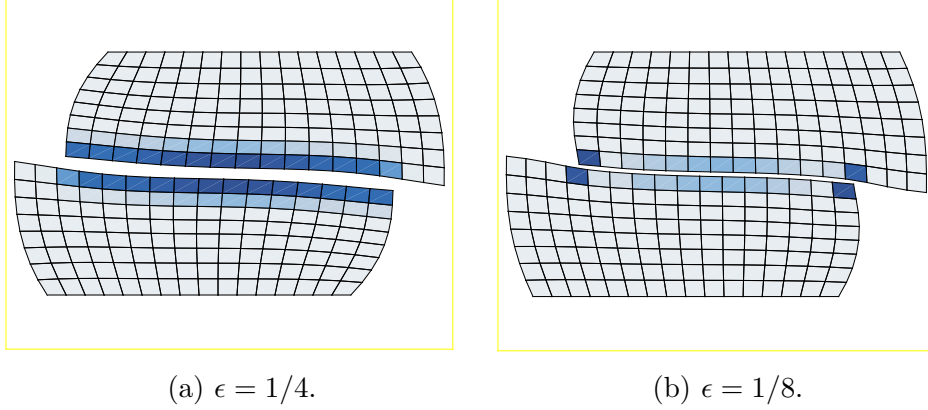


Figure 15: Optimized deformed domains with underlying marginal density of $E_\epsilon^{CN}(y)$ for two values of ϵ . Taken from [46].

4.2 Non-penetrability of elastic solids

A nonpenetration constraint translates into global injectivity of the deformation map $y : \Omega \rightarrow \mathbb{R}^d$ mapping the “reference configuration” $\Omega \subset \mathbb{R}^d$ to the deformed state. The global injectivity of y in suitable spaces of orientation-preserving deformations, i.e., $\det(\nabla y) > 0$ almost everywhere, is equivalent to the well-known Ciarlet-Nečas condition [22]

$$\int_{\Omega} |\det(\nabla y)| \, dx \leq |y(\Omega)|. \quad (4.10)$$

As no rigorous and computationally feasible projection on the constraint (4.10) is known, a penalty method is applied. The bulk version of the penalty is introduced in [46]. It is given as follows:

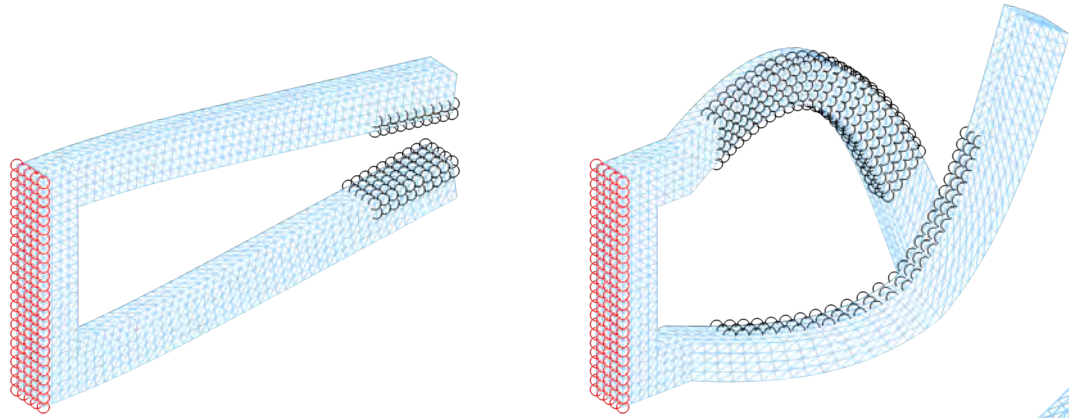
$$E_\epsilon^{CN}(y) := \frac{1}{\epsilon^\beta} \int_{\Omega} d_{\epsilon,y}^{CN}(x) \, dx \quad \text{with} \quad (4.11)$$

$$d_{\epsilon,y}^{CN}(x) := \int_{\Omega} \frac{1}{\epsilon^d} \left[g(|\tilde{x} - x|) - g\left(\frac{|y(\tilde{x}) - y(x)|}{\epsilon}\right) \right]^+ \, d\tilde{x},$$

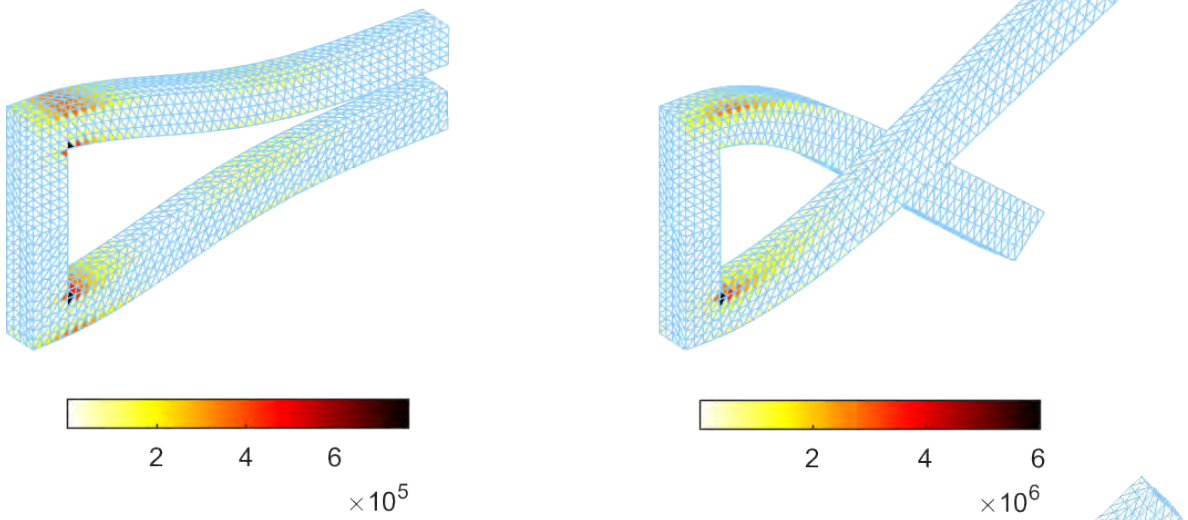
where $[a]^+ := \max\{0, a\}$ denotes the positive part, $\beta > 0$ is a constant and $g : [0, \infty) \rightarrow [0, \infty)$ is a continuous, strictly increasing function with $g(0) = 0$. For locally bi-Lipschitz deformations y , as $\epsilon \rightarrow 0$, $E_\epsilon^{CN}(y)$ converges to zero whenever y satisfies the Ciarlet-Nečas condition (4.10) and is outside self-contact, and to $+\infty$ if (4.10) is violated.

The practical calculation of FEM (cf. Figure 15) involves the minimization of an energy over all feasible deformations. The energy contains the sums of the penalty term, a general function of the gradient (eg., hyperelastic) and a convex function of the second gradient [38]. It is computationally demanding, since the penalty term represents a double integral over Ω . Furthermore, the second gradient evaluation requires the use of non-standard elements C^1 [77].

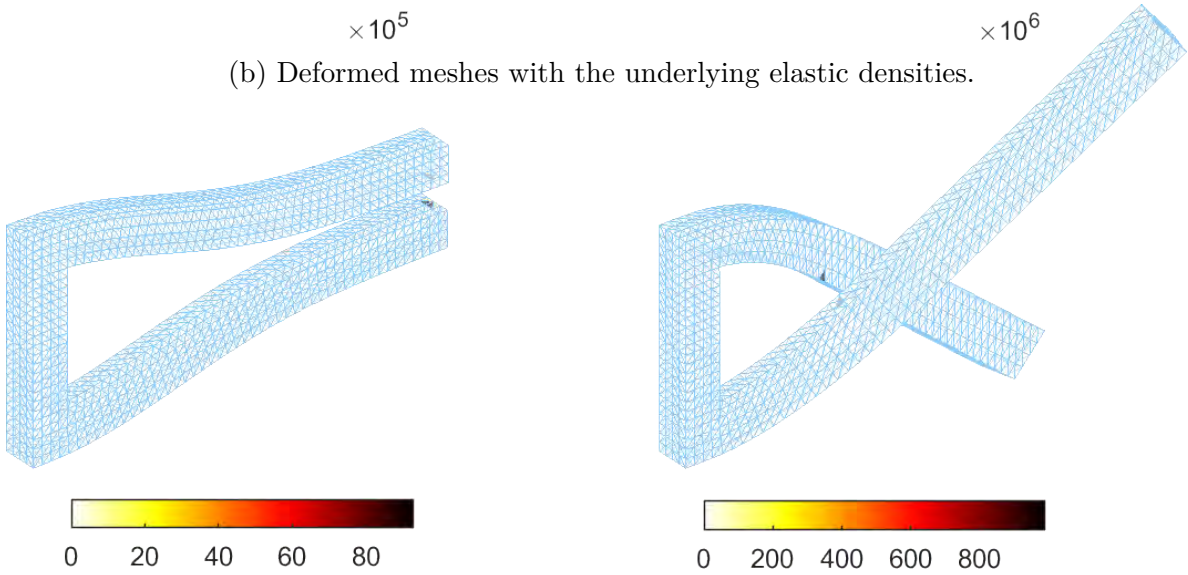
One of the disadvantages of E_ϵ^{CN} is its nonlocal nature and the ensuing computational complexity for numerical evaluation: typically, a single evaluation of the double integral has a cost of the order of elementary operations h^{-2d} , where h is the size of the grid and d the dimension of the reference configuration Ω . Although the nonlocal nature of global invertibility will also be reflected in any associated penalty term, the computational cost can be reduced if we work with integration over the boundary $\partial\Omega$ instead of the full domain, effectively decreasing the dimension.



(a) Initially deformed meshes.



(b) Deformed meshes with the underlying elastic densities.



(c) Deformed meshes with the underlying nonpenetration densities.

Figure 16: Solutions for level 2 mesh: the symmetric initial deformation (the left column) and the asymmetric initial deformation (the right column). Taken from [47].

This is possible while retaining the main effect of the penalty term, using the following surface variant from [47]:

$$\begin{aligned} E_\varepsilon^{\partial\Omega}(y) &:= \frac{1}{\varepsilon^\beta} \int_{\partial\Omega} d_{\varepsilon,y}^{\partial\Omega}(x) \, d\mathcal{H}^{d-1}(x) \quad \text{with} \\ d_{\varepsilon,y}^{\partial\Omega}(x) &:= \int_{\partial\Omega} \frac{1}{\varepsilon^{d-1}} P \left(g(|\tilde{x} - x|) - g\left(\frac{|y(\tilde{x}) - y(x)|}{\varepsilon}\right) \right) d\mathcal{H}^{d-1}(\tilde{x}), \end{aligned} \quad (4.12)$$

where $\beta > d - 1$, g satisfies conditions as before, \mathcal{H}^{d-1} denotes the $(d - 1)$ -dimensional Hausdorff measure (the surface measure) and P is an approximation of the positive part $[\cdot]^+$ in the sense that $P : \mathbb{R} \rightarrow [0, \infty)$ is continuous with $[t - 1]^+ \leq P(t) \leq [t]^+$, and $P(t) > 0$ for $t > 0$. In practice, we choose P and g as smooth approximations of the map $t \mapsto [t]^+$.

To be able to compute 3D benchmarks (cf. Figure 16b), we consider a linear elasticity material combined with the surface penalty only and dropping the second gradient term. Then, the selected nodes (indicated by a black color) are the only unknown in the minimization process. The location of all other nodes is calculated from a linear system of equations corresponding to the linear elasticity.

4.3 Energy minimizations: implementation concepts

Various applications in the calculus of variations aim to solve a minimization problem

$$J(u) = \min_{v \in V} J(v), \quad (4.13)$$

where $J : V \rightarrow \mathbb{R}$ represents an energy functional. As an example we mention the minimization of the p-Laplace energy

$$J(v) := \frac{1}{\alpha} \int_{\Omega} \|\nabla v\|^\alpha \, dx - \int_{\Omega} f v \, dx$$

over the space $V = W_g^{1,\alpha}(\Omega) = \{v \in W^{1,\alpha}, v = g \text{ on } \partial\Omega\}$ assuming that $f \in L^2(\Omega)$ and $g \in W^{1-1/\alpha,\alpha}(\partial\Omega)$. Then, there is a unique minimizer $u \in V$ for the power $\alpha > 1$. Direct minimization (4.13) is an alternative to treating the corresponding Lagrange-Euler equations represented by the well-known p-Laplace equation in this example.

The minimizer can be approximated numerically, see Figure 17. A trial function $v \in V$ is discretized in the finite element space $V_h \subset V$ spanned by a set of n_b basis functions $\varphi_i(x) \in V_h$, $i = 1, \dots, n_b$, where n_b denotes the number of basis functions. It is expressed by a linear combination $v(x) = \sum_{i=1}^{n_b} v_i \varphi_i(x)$, $x \in \Omega$, with a vector of coefficients

$$\underline{v} = (v_1, \dots, v_{n_b}) \in \mathbb{R}^{n_b}.$$

Then a direct minimization (4.13) results in a discrete minimization problem

$$J(\underline{u}_h) = \min_{\underline{v} \in \mathbb{R}^{n_b}} J(\underline{v}). \quad (4.14)$$

The minimizer $u_h \in V_h$ of (4.14) is represented by a vector of coefficients

$$\underline{u}_h = (u_1, \dots, u_{n_b}) \in \mathbb{R}^{n_b}$$

and some coefficients of $\underline{v}, \underline{u}_h$ related to Dirichlet boundary conditions are prescribed.

Unconstrained optimization methods are combined with FEM implementations [5, 66] to solve (4.14) efficiently. These are

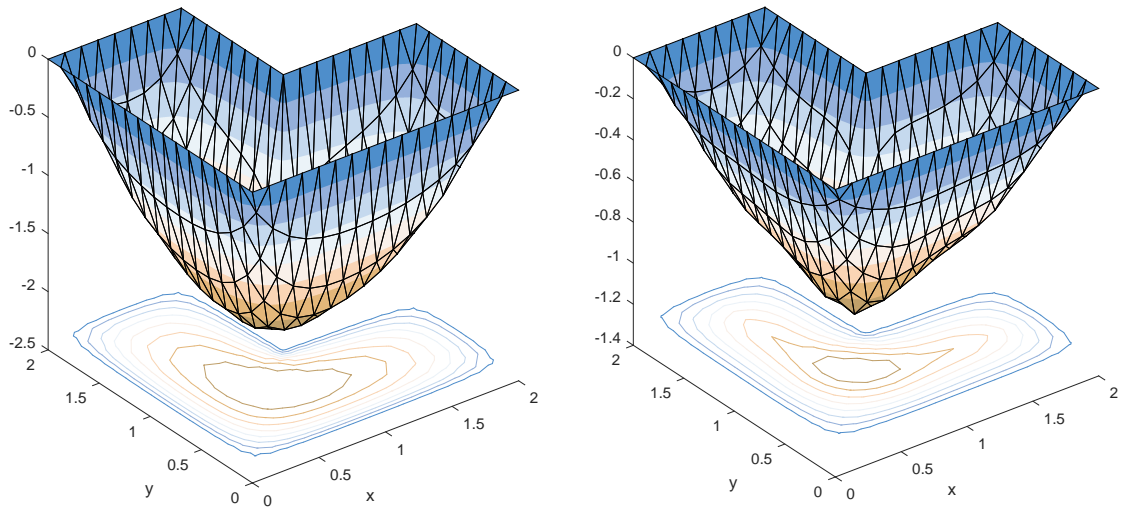


Figure 17: Numerical solutions for $\alpha = 1.8$ (left), $\alpha = 3$ (right) and a L-shape domain Ω , $f = -10$ and zero Dirichlet boundary conditions on $\partial\Omega$. Taken from [54].

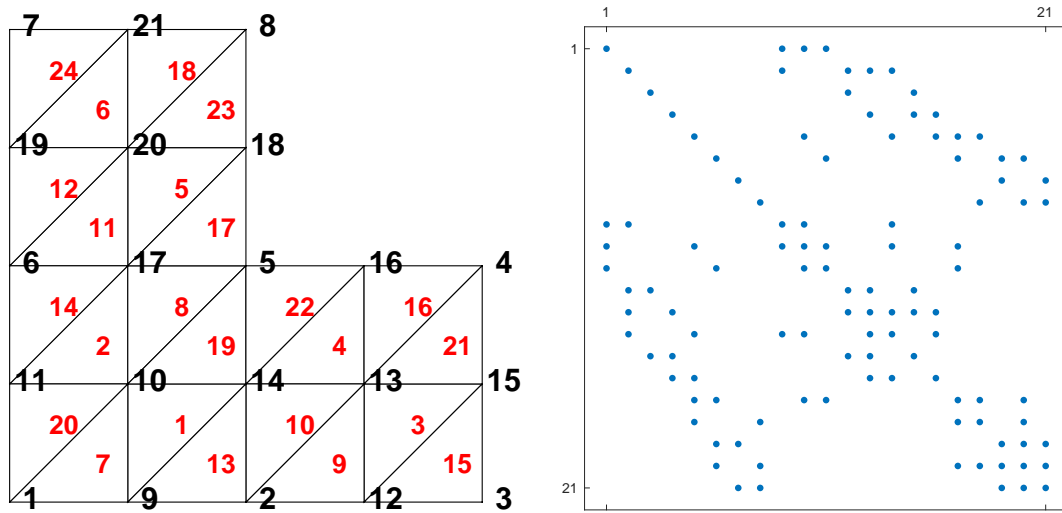


Figure 18: A triangular mesh (left) and the corresponding Hessian sparsity pattern (right). The black and red numbers denote the nodes and elements indices. Taken from [54].

level	free dofs	exact gradient			numerical gradient		
		time [s]	TR-iters	$J(\underline{u}_h)$	time [s]	TR-iters	$J(\underline{u}_h)$
1	33	0.02	10	-7.5353	0.03	10	-7.5353
2	161	0.06	13	-7.9729	0.10	12	-7.9729
3	705	0.12	13	-8.1039	0.21	12	-8.1039
4	2945	0.34	13	-8.1445	0.50	11	-8.1445
5	12033	1.36	13	-8.1578	2.10	12	-8.1578
6	48641	6.95	14	-8.1625	12.56	17	-8.1625
7	195585	52.75	15	-8.1642	78.56	19	-8.1642
8	784385	645.22	24	-8.1649	754.91	24	-8.1649

Table 5: Performance of the TR method for p-Laplacian minimizations ($\alpha = 3$) in 2D. Taken from [57].

the quasi-Newton method (QN)

the trust-region methods (TR)

that are available in the MATLAB Optimization Toolbox. The QN method only requires the knowledge of the function

$$J(\underline{v}), \quad \underline{v} \in \mathbb{R}^{n_b}. \quad (4.15)$$

The TR method [19] additionally needs knowledge of the gradient vector

$$\nabla J(\underline{v}) \in \mathbb{R}^{n_b}, \quad \underline{v} \in \mathbb{R}^{n_b}, \quad (4.16)$$

and allows to specify a sparsity pattern of the Hessian matrix

$$\nabla^2 J(\underline{v}) \in \mathbb{R}^{n_b \times n_b}, \quad \underline{v} \in \mathbb{R}^{n_b}, \quad (4.17)$$

i.e., only positions (indices) of nonzero entries. Note that the Hessian matrix itself is not input by the user, but computed internally instead. The sparsity pattern is provided directly by the finite-element discretization. Fig. 18 shows an example of the triangulation of an L-shaped domain with the corresponding Hessian sparsity. The gradient vector $\nabla J(\underline{v})$ in the trust region methods can be provided analytically by using the chain rule or numerically approximated by the central difference scheme. The latter option is simpler for the user and not significantly slower; see Table 5.

Remark 4.2 *Recent work [12] focuses on the accelerated solution of minimization problems of [57] in Python. It uses the following additional techniques:*

1. *the automatic differentiation tool for computing both the gradient and the Hessian of the energy functional,*
2. *the Newton method with line search using the golden section method,*
3. *algebraic multigrid solver (AMG) to solve linear systems,*
4. *XLA (Accelerated Linear Algebra) compiler to improve the efficiency of computations with objects that are memory costly.*

The speedup of computations is significant (at least 10) for large problems with around several hundred thousands of degrees of freedom (dofs).

Conclusion and outlooks

Section 4 is based on journal articles [10, 46, 47, 57]. The first three articles provide theoretical results from the calculus of variations and complementary computations by the finite element method. We recall that parts of the proofs of [10] were independently verified by our FEM codes, e.g., Proposition 4.8 a). Other contributions to nonlinear problems not reported in this section are

elastoplasticity in small strains with damage [70, 71],

magnetic hysteresis with thermal effects [50],

shape memory alloys [31],

viscoelasticity [26, 30],

elastoplastic deformations of layered structures [27].

Theoretical communities in the calculus of variations are primarily interested in direct energy minimizations rather than solutions of the corresponding Lagrange-Euler equations. Article [57] allows for automatic minimization of nonlinear energetic formulations containing the gradient operator. There is still a large space for efficiency improvements and the need to combine finite elements with existing optimization methods in the future.

5 References

- [1] AXELSSON O.: Iterative Solution Methods, Cambridge University Press, 1996.
- [2] AXELSSON, O., LUKÁŠ, D.: Preconditioning methods for eddy-current optimally controlled time-harmonic electromagnetic problems, *Journal of Numerical Mathematics* **27**, No. 1, 1–21, 2019.
- [3] ALBERTY J., CARSTENSEN C. AND FUNKEN S. A.: Remarks around 50 lines of Matlab: short finite element implementation. *Numerical Algorithms* **20**, 117–137, 1999.
- [4] ALBERTY J., CARSTENSEN C., FUNKEN, S. A., AND KLOSE R.: Matlab implementation of the finite element method in elasticity. *Computing* **69**, No. 6, 236–263, 2002.
- [5] ANJAM I., VALDMAN J.: Fast MATLAB assembly of FEM matrices in 2D and 3D: edge elements, *Applied Mathematics and Computation* **267**, 252–263, 2015.
- [6] BADER B. W., KOLDA T. G.: Algorithm 862: MATLAB Tensor Classes for Fast Algorithm Prototyping, *ACM Trans. Mathematical Software*, *32*, No. 4:635–653, 2006.
- [7] BANGERTH W., RANNACHER R.: Adaptive Finite Element Methods for Differential Equations, Springer, 2003.
- [8] BARTELS S.: Numerical methods for nonlinear partial differential equations, Springer, 2015.
- [9] BATHE K. J.: Finite-Element Procedures, Klaus-Jürgen Bathe, 2006.
- [10] BEVAN J., KRUŽÍK M., VALDMAN J.: Hadamard’s inequality in the mean, *Nonlinear Analysis* **243**, 2023.
- [11] BEVAN J., KRUŽÍK M., VALDMAN J.: Using mean Hadamard inequalities to determine incompressible, global energy minimizers (in preparation).
- [12] BÉREŠ M., VALDMAN J.: Minimization of Nonlinear Energies in Python Using FEM and Automatic Differentiation Tools, PPAM 2024, Lecture Notes in Computer Science (accepted).

- [13] BROKATE M., CARSTENSEN C., VALDMAN J.: A Quasi-Static Boundary Value Problem in Multi-Surface Elastoplasticity. Part I: Analysis. *Math. Meth. Appl. Sciences* **27**, No. 14, 1697–1710, 2004.
- [14] BROKATE M., CARSTENSEN C., VALDMAN J.: A Quasi-Static Boundary Value Problem in Multi-Surface Elastoplasticity. Part II: Numerical Solution. *Math. Meth. Appl. Sciences* **28**, No. 14, 881–901, 2005.
- [15] BOFFI, D.: Finite element approximation of eigenvalue problems, *Acta Numerica*, pp. 1–120 (2010).
- [16] BOZORGNIA F., VALDMAN J.: A FEM approximation of a two-phase obstacle problem and its a posteriori error estimate, *Computers & Mathematics with Applications* **73**, No. 3, 419–432, 2017.
- [17] CAFFARELLI L.: The obstacle problem revisited. *The Journal of Fourier Analysis and Applications* **4**, 383–402, 1998.
- [18] CARSTENSEN C., FEISCHL M., PAGE M., PRAETORIUS D.: Axioms of adaptivity, *Computers and Mathematics with Applications* **67**, 1195–1253, 2014.
- [19] CONN A. R., GOULD N. I. M., TOINT P. L.: Trust-Region Methods, SIAM, Philadelphia, 2000.
- [20] COURANT R.: Variational methods for the solution of problems of equilibrium and vibrations, *Bulletin of the American Mathematical Society*, **43**, No. 1, 1943.
- [21] CIARLET P.G.: The finite element method for elliptic problems. North-Holland, Amsterdam, 1978.
- [22] CIARLET P., NEČAS J.: Injectivity and self-contact in nonlinear elasticity, *Archive for Rational Mechanics and Analysis* **97**, 173–188, 1987.
- [23] ČERMÁK M., KOZUBEK T., SYSALA S., VALDMAN J.: A TFETI Domain Decomposition Solver for Elastoplastic Problems, *Applied Mathematics and Computation* **231**, 634–653, 2014.
- [24] ČERMÁK M., SYSALA S., VALDMAN J.: Efficient and flexible MATLAB implementation of 2D and 3D elastoplastic problems, *Applied Mathematics and Computation* **355**, 595–614, 2019.
- [25] DACOROGNA B.: Direct Methods in the Calculus of Variations. 2nd ed. Springer Science+Business Media, 2008.
- [26] DONDL P., JESENKO M., KRUŽÍK M., VALDMAN J.: Linearization and Computation for Large-Strain Viscoelasticity, *Mathematics in Engineering* **5**, No. 2: 1–15, 2023.
- [27] DROZDENKO D., KRUŽÍK M., KNAPEK M., MÁTHIS K., ŠVADLENKA K, VALDMAN J.: Elastoplastic deformations of layered structures, *Milan Journal of Mathematics* **90**, No. 2, 691–706, 2022.
- [28] EVANS L. C.: Partial differential equations, 2nd ed. American Mathematical Society, 2010.
- [29] FIX G., STRANG G.: An Analysis of the Finite Element Method, Wellesley-Cambridge Press, 2008.
- [30] FRIEDRICH M., KRUŽÍK M., VALDMAN J.: Numerical approximation of von Kármán viscoelastic plates, *Discrete and Continuous Dynamical Systems, Series S* **14**, No. 1, 299–319, 2021.
- [31] FROST M., KRUŽÍK M., VALDMAN J.: Interfacial polyconvex energy-enhanced evolutionary model for shape memory alloys, *Mathematics and Mechanics of Solids* **24**, No. 8, 2619–2635, 2019.
- [32] FROST M., MOSKOVKA A., VALDMAN J.: Minimization of energy functionals via FEM: implementation of hp-FEM, I. Lirkov and S. Margenov (eds): LSSC 2023, 2024.
- [33] FROST M., VALDMAN J.: Vectorized MATLAB Implementation of the Incremental Minimization Principle for Rate-Independent Dissipative Solids Using FEM: A Constitutive Model of Shape Memory Alloys, *Mathematics* **10**, 4412, 2022.

- [34] FRUTOS J.M., ESPARZA F.P.: Optimal Control of PDEs under Uncertainty. An Introduction with Application to Optimal Shape Design of Structures, SpringerBriefs in Mathematics, Springer 2018.
- [35] FUNKEN S., PRAETORIUS D., WISSGOTT, P.: Efficient implementation of adaptive P1-FEM in Matlab, *Computational Methods in Applied Mathematics* **11**, No. 4, 460–490, 2011.
- [36] GRUBER P., VALDMAN J.: Solution of one-time-step problems in elastoplasticity by a Slant Newton Method, *SIAM Journal on Scientific Computing* **31**, No. 2, 1558–1580, 2009.
- [37] GFREERER H., MANDLMAYR M., OUTRATA J.V., VALDMAN J.: On the SCD semismooth* Newton method for generalized equations with application to a class of static contact problems with Coulomb friction. *Computational Optimization and Applications* **86**, 1159–1191, 2023.
- [38] HEALEY T. J., KRÖMER S.: Injective weak solutions in second-gradient nonlinear elasticity. *ESAIM: COCV* **15**, 863–871, 2009.
- [39] HAN W., REDDY B.: Plasticity: Mathematical Theory and Numerical Analysis. Springer-Verlag New York, 1999.
- [40] HIPTMAIR R.: Symmetric coupling for eddy current problems. *SIAM Journal on Numerical Analysis* **40**, 41–65, 2002.
- [41] HRENNIKOFF A.: Solution of Problems of Elasticity by the Frame-Work Method. *ASME J. Appl. Mech.* **8**, A619–A715, 1944.
- [42] HRUBÝ F.: GPU Computing capabilities in MATLAB, Bc. Thesis, in Czech, University of South Bohemia, České Budějovice, Czech Republic, 2022.
- [43] KINDERLEHRER D., STAMPACCHIA G.: An Introduction to Variational Inequalities and Their Applications. *Academic Press*, 1980.
- [44] KRAUS, J., MARGENOV, S.: Robust Algebraic Multilevel Methods and Algorithms, De Gruyter Berlin-New York, 2009.
- [45] KRIEZIS E. E., TSIBOUKIS T. D., PANAS S. M. AND TEGOPOULOS J. A.: "Eddy currents: theory and applications," in Proceedings of the IEEE, vol. 80, no. 10, pp. 1559-1589, Oct. 1992.
- [46] KRÖMER S., VALDMAN J.: Global injectivity in second-gradient Nonlinear Elasticity and its approximation with penalty terms, *Mathematics and Mechanics of Solids* **24**, No. 11, 3644–3673, 2019.
- [47] KRÖMER S., VALDMAN J.: Surface penalization of self-interpenetration in linear and nonlinear elasticity, *Applied Mathematical Modelling* **122**, 641–664, 2023.
- [48] KRUŽÍK M., ROUBÍČEK T.: Mathematical Methods in Continuum Mechanics of Solids, Springer, 2019.
- [49] KŘÍŽEK, M., NEITTAANMÄKI P.: Mathematical and Numerical Modelling in Electrical Engineering Theory and Applications, Springer, 1996.
- [50] KRUŽÍK M., VALDMAN J.: Computational modeling of magnetic hysteresis with thermal effects, *Mathematics and Computers in Simulation* **145**, 90–105, 2018.
- [51] LIU W.K., LI S., PARK H.S.: Eighty Years of the Finite Element Method: Birth, Evolution, and Future. *Archives of Computational Methods in Engineering* **29**, 4431–4453, 2022.
- [52] LI J.R., NGUYEN V.D., TRAN T.N., VALDMAN J., TRANG B.C., NGUYEN K.V., SON V.D.T., TRAN H.A., TRAN H.A.T., NGUYEN T.M.P: SpinDoctor: a Matlab toolbox for diffusion MRI simulation, *Neuroimage* **202**, pages 116120, 2019.

- [53] MARCINKOWSKI L., VALDMAN J.: MATLAB Implementation of Element-based Solvers, I. Lirkov and S. Margenov (eds): LSSC 2019, LNCS 11958, pp. 601–609 (2020).
- [54] MATONOHA C., MOSKOVKA A., VALDMAN J.: Minimization of p-Laplacian via the Finite Element Method in MATLAB, LSSC 2021, Lecture Notes in Computer Science (LNCS) 13127, pp. 533-540 (2022).
- [55] MONK P.: Finite element methods for Maxwell’s equations, Oxford University Press, 2003.
- [56] MOSKOVKA A., RAHMAN T., VALDMAN J., VATNE J. E.: On a vectorized basic linear algebra package for prototyping codes in MATLAB (in preparation).
- [57] MOSKOVKA A., VALDMAN J.: Fast MATLAB evaluation of nonlinear energies using FEM in 2D and 3D: nodal elements, *Applied Mathematics and Computation* **424**, 127048, 2022.
- [58] MOSKOVKA A., VALDMAN J.: MATLAB implementation of hp finite elements on rectangles using hierarchical basis functions, PPAM 2022, Lecture Notes in Computer Science (LNCS) 13827, pp. 287–299, 2023.
- [59] MOSKOVKA A., VALDMAN J., VOHNOUTOVÁ M.: On Minimization of Nonlinear Energies Using FEM in MATLAB, PPAM 2022, Lecture Notes in Computer Science (LNCS) 13827, pp. 331–342, 2023.
- [60] NÉDÉLEC J. C.: Mixed finite elements in \mathbb{R}^3 . *Numerische Mathematik* **35**, 315–341, 1980.
- [61] NEITTAANMÄKI P., REPIN S.: Reliable methods for computer simulation. Error control and a posteriori estimates. *Elsevier*, volume 33, 2004.
- [62] NEITTAANMÄKI P., REPIN S., VALDMAN J.: Estimates of deviations from exact solutions of elasticity problems with nonlinear boundary conditions, *Russian Journal of Numerical Analysis and Mathematical Modelling* **28**, No. 6, 597–630, 2013
- [63] OUTRATA J., KOČVARA M., ZOWE J.: Nonsmooth Approach to Optimization Problems with Equilibrium Constraints, Kluwer, (Dordrecht 1998) Nonconvex Optimization and Its Applications. vol.28, 1998.
- [64] DE SOUZA NETO E.A., PERIC D., OWEN D.R.J.: Computational Methods for Plasticity, Wiley-Blackwell, 2008.
- [65] PAULY D., VALDMAN, J.: Friedrichs/Poincare Type Constants for Gradient, Rotation, and Divergence: Theory and Numerical Experiments, *Computers & Mathematics with Applications* **79**, No. 11, 3027–3067, 2020.
- [66] RAHMAN T., VALDMAN J.: Fast MATLAB assembly of FEM matrices in 2D and 3D: nodal elements, *Applied Mathematics and Computation* **219**, No. 13, 7151–7158, 2013.
- [67] RAVIART P.A., THOMAS J.M.: A mixed finite element method for 2-nd order elliptic problems. In: Galligani, I., Magenes, E. (eds) *Mathematical Aspects of Finite Element Methods*. Lecture Notes in Mathematics, volume 606. Springer, Berlin, Heidelberg, 1977.
- [68] REPIN S., VALDMAN J.: Functional a posteriori error estimates for problems with nonlinear boundary conditions, *Journal of Numerical Mathematics* **16**, No. 1, 51–81, 2008.
- [69] REPIN S., VALDMAN J.: Error identities for variational problems with obstacles, *ZAMM - Journal of Applied Mathematics and Mechanics, Zeitschrift für Angewandte Mathematik und Mechanik* **98**, No. 4, 635–658, 2018.

- [70] ROUBÍČEK T., VALDMAN J.: Perfect plasticity with damage and healing at small strains, its modelling, analysis, and computer implementation, *SIAM Journal on Applied mathematics* **76**, No. 1, 314–340 (2016).
- [71] ROUBÍČEK T., VALDMAN J.: Stress-driven solution to rate-independent elasto-plasticity with damage at small strains and its computer implementation, *Mathematics and Mechanics of Solids* **22**, No. 6, 1267–1287 (2017).
- [72] SCHÖBERL J., ZAGLMAYR S.: High order Nédélec elements with local complete sequence properties, *COMPEL - The international journal for computation and mathematics in electrical and electronic engineering*, 2005.
- [73] SHAHGHOLIAN H., URALTSEVA N. N., WEISS. G. S.: The two-phase membrane problem – regularity of the free boundaries in higher dimensions. *International Mathematics Research Notices*, volume 2007, 2007.
- [74] SZABÓ B., BABUŠKA I.: Introduction to Finite Element Analysis, John Wiley & Sons, 2011.
- [75] SIMO J.C., HUGHES T.J.R.: Computational Inelasticity, Springer-Verlag, 1998.
- [76] VALDMAN J.: Minimization of Functional Majorant in A Posteriori Error Analysis based on H(div) Multigrid-Preconditioned CG Method, *Advances in Numerical Analysis*, vol. 2009, Article ID 164519, 2009.
- [77] VALDMAN J.: MATLAB Implementation of C1 finite elements: Bogner-Fox-Schmit rectangle, In: Wyrzykowski R., Deelman E., Dongarra J., Karczewski K. (eds) Parallel Processing and Applied Mathematics. PPAM 2019. Lecture Notes in Computer Science, vol 12044. Springer, Cham, 2020.
- [78] VALDMAN J.: Mathematical and Numerical Analysis of Elastoplastic Material with Multi-Surface Stress-Strain Relation. *Verlag dissertation.de* (2002), Berlin, ISBN 3-89825-501-8.
- [79] VALDMAN J.: On Modeling and A Posteriori Error Estimates for some Convex Problems in Continuum Mechanics. TU Ostrava, Czech Republic, (2010) submitted, (2011) defended.